Cell Reports
Medicine

Article

Potentiating anti-tumor immunity by re-engaging immune synapse molecules

Graphical abstract

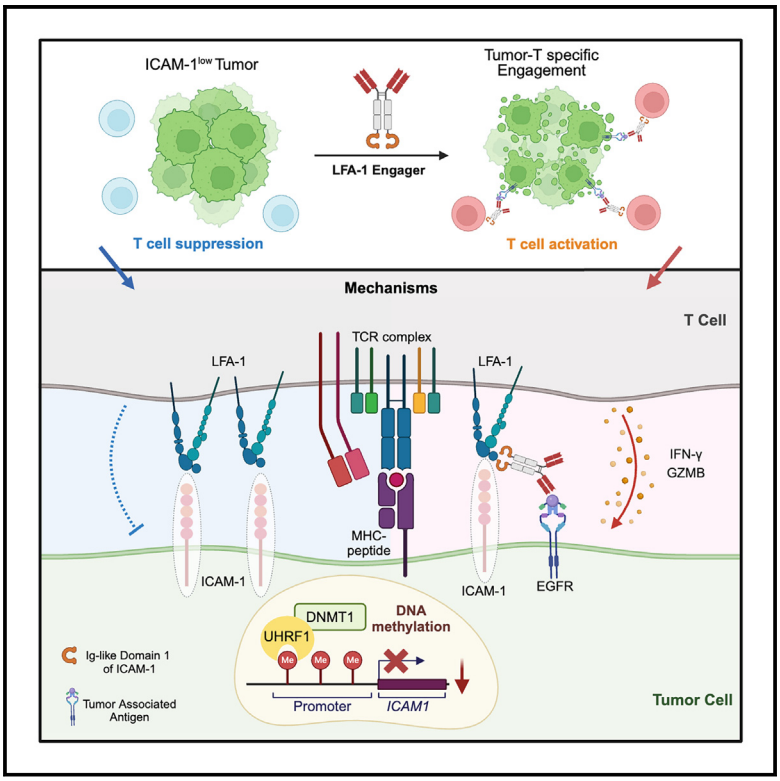

Highlights

- Absence of ICAM-1 drives tumor resistance to T and NK cell-mediated killing
- Tumor ICAM-1 is repressed by UHRF1/DNMT1-mediated DNA methylation
- LFA-1 engager restores ICAM-1 signaling and enhances T cell cytotoxicity
- LFA-1 engager boosts anti-tumor immunity and synergizes with ICB therapies

Authors

Xindi Zhou, Tian Xu, Changhe Li, ..., Yangxin Fu, Zexian Zeng, Deng Pan

Correspondence

zexianzeng@pku.edu.cn (Z.Z.), dpan@tsinghua.edu.cn (D.P.)

In brief

Zhou et al. reveal that DNA methylation-driven ICAM-1 loss confers tumor resistance to T and NK cell killing. Restoring ICAM-1/LFA-1 signaling with "LFA-1 engager" enhances anti-tumor immunity and boosts immune checkpoint blockade efficacy, presenting a promising therapeutic strategy for ICAM-1-deficient tumors.

Zhou et al., 2025, Cell Reports Medicine 6, 101975
March 18, 2025
https://doi.org/10.1016/j.xcrm.2025.101975

CellPress

Cell Reports Medicine

CellPress
OPEN ACCESS

Article

Potentiating anti-tumor immunity by re-engaging immune synapse molecules

Xindi Zhou,[1] Tian Xu,[2] Changhe Li,[1] Yufeng He,[2] Yuanzhi Hu,[1] Hao Gong,[1] Jiahui Li,[1] Haitao Jiang,[1] Liang Wen,[5] Yangxin Fu,[1] Zexian Zeng,[2,4,*] and Deng Pan[1,3,6,*]

[1]State Key Laboratory of Molecular Oncology, School of Basic Medical Sciences, Tsinghua University, Beijing 100084, China
[2]Peking-Tsinghua Center for Life Sciences, Academy for Advanced Interdisciplinary Studies, Peking University, Beijing 100871, China
[3]Tsinghua-Peking Center for Life Science (CLS), Beijing 100084, China
[4]Center for Quantitative Biology, Academy for Advanced Interdisciplinary Studies, Peking University, Beijing 100871, China
[5]Chinese People's Liberation Army (PLA) Medical School, Beijing 100850, China
[6]Lead contact
*Correspondence: zexianzeng@pku.edu.cn (Z.Z.), dpan@tsinghua.edu.cn (D.P.)
https://doi.org/10.1016/j.xcrm.2025.101975

SUMMARY

The formation of immune synapses (ISs) between cytotoxic T cells and tumor cells is crucial for effective tumor elimination. However, the role of ISs in immune evasion and resistance to immune checkpoint blockades (ICBs) remains unclear. We demonstrate that ICAM-1, a key IS molecule activating LFA-1 signaling in T and natural killer (NK) cells, is often expressed at low levels in cancers. The absence of ICAM-1 leads to significant resistance to T and NK cell-mediated anti-tumor immunity. Using a CRISPR screen, we show that ICAM-1 is epigenetically regulated by the DNA methylation pathway involving UHRF1 and DNMT1. Furthermore, we engineer an antibody-based therapeutic agent, "LFA-1 engager," to enhance T cell-mediated anti-tumor immunity by reconstituting LFA-1 signaling. Treatment with LFA-1 engagers substantially enhances immune-mediated cytotoxicity, potentiates anti-tumor immunity, and synergizes with ICB in mouse models of ICAM-1-deficient tumors. Our data provide promising therapeutic strategies for re-engaging immune stimulatory signals in cancer immunotherapy.

INTRODUCTION

Cytotoxic T cells (cytotoxic T lymphocytes [CTLs]) and natural killer (NK) cells are key effectors of the immune system that play a central role in the elimination of tumor cells.[1–3] CTL activation is primarily driven by the interaction of the T cell receptor (TCR) with the major histocompatibility complex (MHC)-peptide complex presented on tumor cells. Similarly, the activation of NK cells is driven by the engagement of major NK-activating receptors, including B7-H6 and natural killer group 2 member D (NKG2D).[4] However, tumors have developed various intrinsic mechanisms to evade recognition and killing by CTLs and NK cells. These mechanisms include the downregulation of MHC expression,[5,6] upregulation of immune inhibitory molecules (e.g., programmed death-ligand 1 [PD-L1] and SPERPINB9),[7–9] downregulation or shedding of major NK-activating ligands (e.g., MHC Class I chain-related protein A/B [MICA/B]),[10] and secretion of immune-suppressive cytokines (e.g., transforming growth factor β) to reprogram the tumor microenvironment,[11] allowing tumors to persist and grow despite the presence of CTLs and NK. The development of strategies to overcome these evasion mechanisms is therefore essential for the success of cancer immunotherapy.

The effective elimination of tumor cells by CTLs and NK cells is critically dependent on the formation of the immune synapse, a specialized interface between the target cells or antigen-presenting cells and T cells. The formation of the immune synapse involves the interaction between lymphocyte function-associated antigen 1 (LFA-1) on T cells and intercellular adhesion molecule 1 (ICAM-1) on target cells. Upon ICAM-1/LFA-1 binding, T cells extend pseudopodia to scan the surface of target cells for specific MHC-peptide complexes, which then activate the TCR.[12–14] This interaction not only facilitates the formation and stabilization of immune synapses between T cells and their target cells but also plays a crucial role in lymphocyte migration to lymphoid tissues and sites of infection and inflammation.[15] Additionally, ICAM-1/LFA-1 interaction could lower the density of antigens and TCR signals necessary for T cell activation and functional response.[16] Despite their vital roles in immune recognition and trafficking, the contributions of ICAM-1/LFA-1 to cancer immune evasion and the potential to manipulate ICAM-1/LFA-1 signaling for cancer therapy remain unclear.

In this study, we show that ICAM-1 expression is frequently low or absent in human and murine cancer cells, presenting an emerging immune evasion mechanism that enables tumor cells to evade eradication by CTLs and NK cells. Through a genome-wide CRISPR-Cas9 screen, we demonstrate that ICAM-1 is regulated through a variety of epigenetic mechanisms, particularly the DNA methylation inheritance pathway orchestrated by Ubiquitin-Like containing PHD and RING fingers

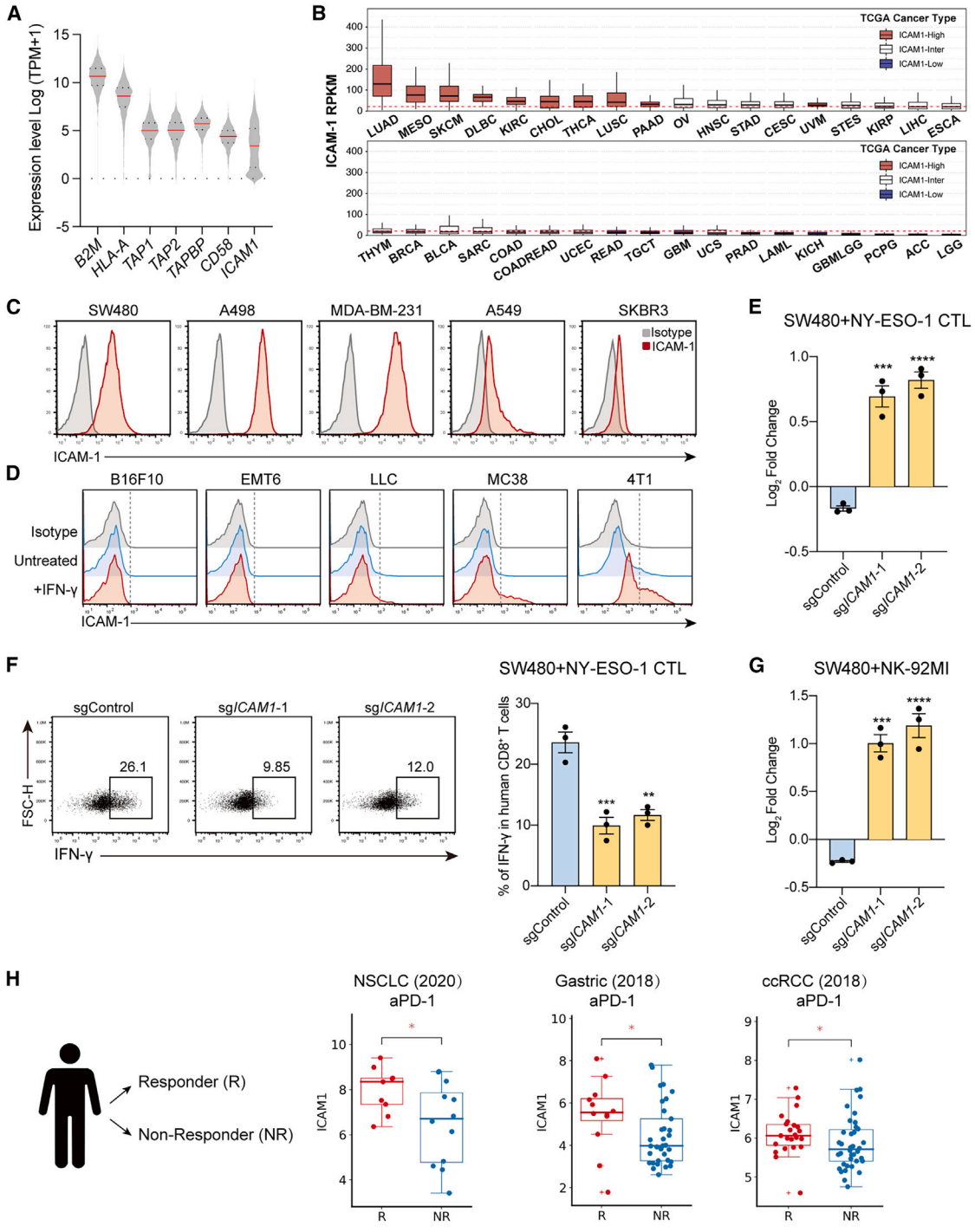

Figure 1. Silencing of ICAM-1 confers resistance to CTL and NK cell-mediated killing

(A) The mRNA expression level of MHC and co-stimulatory molecules among 1,086 human cancer cell lines from the CCLE database.

(B) Pan-cancer analysis of ICAM-1 expression level on different cancer types from TCGA database. ICAM-1 median expression value is show in red line.

(C and D) FACS analysis of surface ICAM-1 level on indicated human (C) and murine (D) cancer cell lines. Murine cells were either untreated or treated with IFN-γ (50 ng/mL) for 24 hours.

(E) *In vitro* competition assay of tumor and CTL co-culture. Control (sgControl) SW480 cells were either mixed with tdTomato-labeled control (sgControl) cells or ICAM-1 KO cells. These mixture cells were then co-cultured with NY-ESO-1-specific T cells or control T cells without the expression of TCR against NY-ESO-1. Log_2 fold changes of the percentage of mixture SW480 cells upon co-culture with NY-ESO-1-specific CTLs as compared with that co-cultured with control T cells were shown ($n = 3$).

(legend continued on next page)

domain 1 (UHRF1) and DNA methyltransferase 1 (DNMT1). In response to the diminished ICAM-1 expression on tumor cells, we developed an innovative antibody-based therapeutic agent, termed "LFA-1 engager," which reconstitutes ICAM-1 signaling on tumor cells. The use of LFA-1 engagers effectively compensates for the absence of ICAM-1, substantially enhancing immune-mediated cytotoxicity and boosting anti-tumor immunity in mouse models. Thus, our results present a promising cancer therapy approach by reactivating the ICAM-1/LFA-1 signaling.

RESULTS

The absence of tumor-intrinsic ICAM-1 confers resistance to both CTL and NK cell-mediated killing

To identify the immune evasion mechanisms that would lead to comprised immune stimulatory signals and the formation of the immune synapse, we analyzed the mRNA expression levels of MHC-I molecules (*B2M*, histocompatibility leukocyte antigen [*HLA*]-*A*, *HLA-B*, and *HLA-C*) and the co-stimulatory/adhesion molecules (*CD58* and *ICAM1*), among 1,086 human cancer cell lines using the Cancer Cell Line Encyclopedia (CCLE) database. Notably, as compared with HLA molecules and CD58, a significant proportion of cancer cells exhibited markedly low expression of ICAM-1, a key immune synapse molecule interacting with the integrin receptor LFA-1 on CTLs and NK cells (Figure 1A). To gain a comprehensive understanding of ICAM-1 expression across different cancers, we performed a pan-cancer analysis using The Cancer Genome Atlas (TCGA) database. Cancer types were categorized into three groups—ICAM-1 high, intermediate, and low expression—based on the median ICAM-1 expression across all samples. Our analysis revealed that many cancer types exhibited high ICAM-1 expression, while others showed intermediate or low levels, reflecting significant variability in ICAM-1 expression across cancer types (Figure 1B). To validate these findings, we assessed ICAM-1 expression by flow cytometry (fluorescence-activated cell sorting [FACS]) using a panel of human cancer cell lines available in our laboratory. We observed variable ICAM-1 expression across these lines. The A549 non-small cell lung cancer (NSCLC) cell line showed detectable ICAM-1 expression, while the MDA-MB-231 triple-negative breast cancer (TNBC) cell line exhibited high levels of ICAM-1 (Figure 1C). In contrast, the SKBR3 breast cancer cell line showed no detectable ICAM-1 expression (Figure 1C). Interestingly, ICAM-1 was undetectable in several murine cell lines, including B16F10, EMT6, Lewis lung carcinoma (LLC), MC38, and 4T1 cells (Figure 1D). Treatment with interferon-gamma (IFN-γ) failed to induce ICAM-1 expression in these murine lines, with the exception of 4T1 cells, which showed an induced response (Figure 1D). These findings suggest that ICAM-1 expression is highly variable both among and within cancer types, with absent or low ICAM-1 expression observed in multiple cancer cell lines.

To investigate the functional relevance of ICAM-1 in immune evasion, we used CRISPR-Cas9 to knock out the *ICAM1* gene in A498 and SW480 cells, both of which express high levels of ICAM-1 (Figures 1C and S1A). Importantly, knockout (KO) of ICAM-1 on A498 and SW480 tumor cells did not result in alterations in tumor growth, morphology, or MHC-I levels compared to control tumor cells (Figures S1B–S1F). We also assessed key differentiation markers, including CD44 and Ep-CAM,[17–19] which showed comparable expression levels between ICAM-1 KO and control cells (Figure S1G). These *ICAM1* KO and control cells were then engineered to express tumor antigen NY-ESO-1 for specific killing mediated by CTLs expressing NY-ESO-1-specific TCR. By using CTLs derived from independent healthy donors, we showed that ICAM-1 KO cells were substantially more resistant to CTL-mediated killing (Figures 1E and S2A–S2E). Consistent with reduced killing phenotype, we also observed a substantial reduction in IFN-γ levels in T cells when co-cultured with ICAM-1 KO cells as compared to control, indicating that ICAM-1/LFA-1 signaling plays a critical role in the effector function of CTLs upon their interaction with tumor cells (Figure 1F). To determine whether restoring ICAM-1 expression could enhance tumor cell sensitivity to CTL-mediated killing, we ectopically expressed *Icam1* in B16F10 cells by utilizing a minimal cytomegalovirus promoter, ensuring its expression remained within a physiologically relevant expression level (Figure S2F). Overexpression of *Icam1* did not change the level of MHC-I (Figure S2G). As expected, overexpression of *Icam1* rendered B16F10 tumors much more sensitive to killing mediated by OT-I and Pmel-1 T cells, respectively (Figures S2H and S2I).

As LFA-1 is also expressed on NK cells, we examined whether ICAM-1 silencing could confer resistance to NK cell-mediated killing. In both A498 and SW480 cell lines, ICAM-1 KO cells were much more resistant to killing mediated by NK-92MI cells (Figures 1G and S2J). Consistently, the levels of CD107a in NK cells were also reduced upon co-culture with ICAM-1 KO cells as compared with control (Figure S2K). Together, these findings collectively suggest that the silencing of ICAM-1 in tumors confers resistance to both CTL and NK cell-mediated killing.

To assess the clinical relevance of ICAM-1 expression and its association with the response to immune checkpoint blockade (ICB), we analyzed published bulk RNA sequencing (RNA-seq) data obtained from tumors collected from patients before they received ICB treatment. We found that in 3 different cohorts from various cancer types,[20–22] the expression of ICAM-1 is significantly lower in non-responders as compared to responders (Figure 1H), suggesting that low expression of ICAM-1 is relevant to resistance of ICB in human cancers.

(F) FACS analysis of intracellular IFN-γ production in NY-ESO-1-specific CTLs upon co-culture with SW480 tumor cells with indicated genotype. Representative FACS (left) and summary (right) showing the percentage of IFN-γ-producing CTLs in the indicated conditions ($n = 3$).
(G) *In vitro* competition assay of tumor and NK-92-MI co-culture. Log_2 fold changes of the percentage of mixture SW480 cells upon co-culture with NK-92MI cells as compared with that without NK-92MI co-culture were shown ($n = 3$).
(H) Tumor ICAM-1 expression levels of the responders and non-responders of ICB were shown in the indicated clinical cohorts.
Data are presented as means ± SEM (E–G). $^{*}p < 0.05$, $^{**}p < 0.01$, $^{***}p < 0.001$, and $^{****}p < 0.0001$ by one-way ANOVA (E–G). Data are representative of at least two independent experiments (C–G).

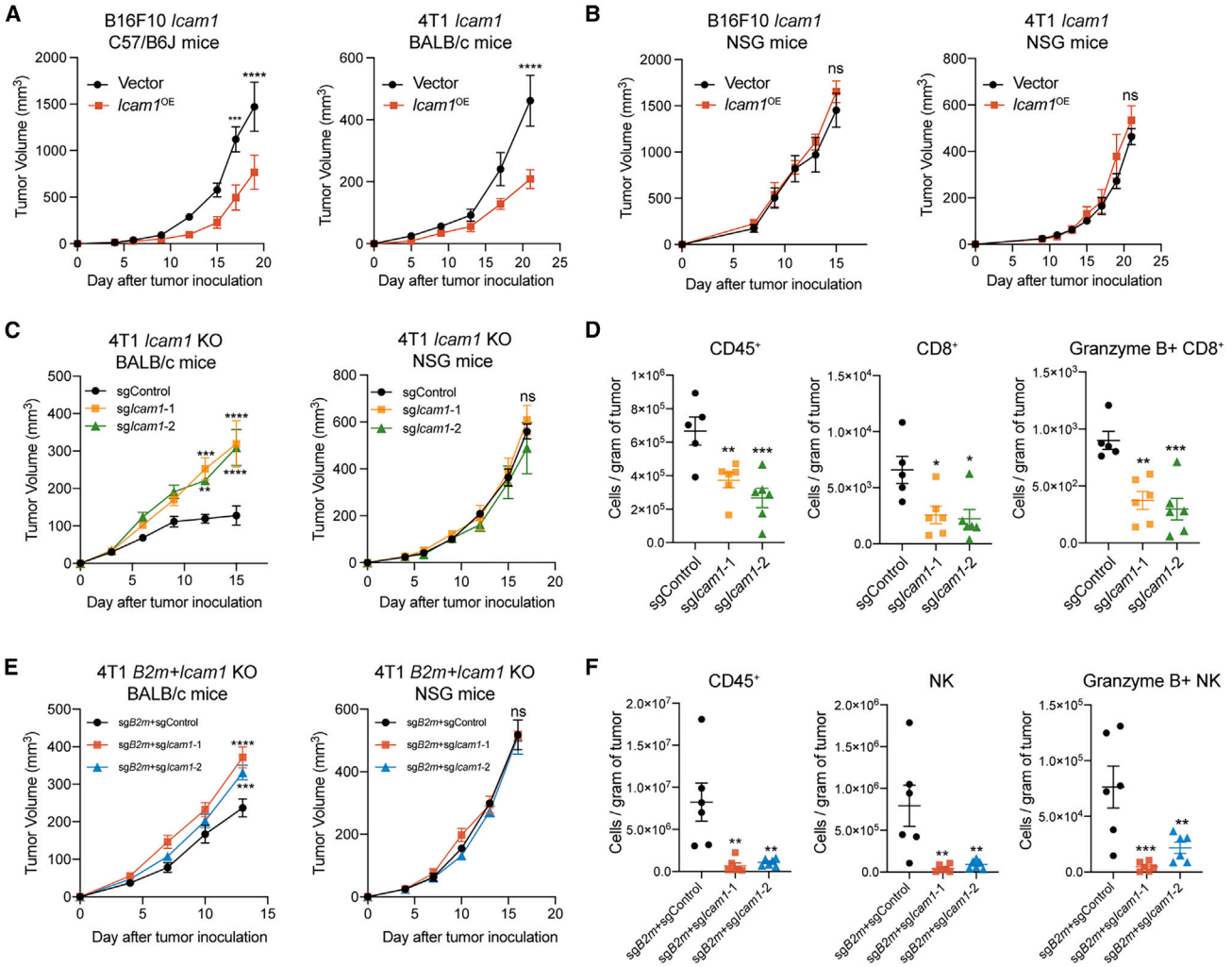

Figure 2. Tumor-intrinsic ICAM-1 is critical for immune evasion for both MHC-I-sufficient and deficient tumors

(A and B) Vector-transduced or *Icam1*^{OE} B16F10 and 4T1 tumors were inoculated in wild-type mice (A) and NSG mice (B), respectively. Tumor growth curves were recorded and shown. n = 5–6 mice per group.

(C) Control (sgControl) and *Icam1* KO (sg*Icam1*) 4T1 tumors were inoculated in the wild-type and NSG mice, respectively. Tumor growth curves were recorded and shown. n = 4–5 mice per group.

(D) Summary of FACS analysis comparing the number of indicated tumor-infiltrating immune cells between control and *Icam1* KO 4T1 tumors on day 16 after tumor inoculation (n = 5–6).

(E) *B2m*/*Icam1* double KO (sg*B2m* + sg*Icam1*) or *B2m* single KO (sg*B2m* + sgControl) 4T1 tumors were inoculated in the wild-type and NSG mice, respectively. Tumor growth curves were recorded and shown. n = 4–6 mice per group.

(F) Summary of FACS analysis comparing the number of indicated tumor-infiltrating immune cells between *B2m*/*Icam1* double KO and *B2m* single KO 4T1 tumors on day 15 after tumor inoculation (n = 6).

Data are presented as means ± SEM (A–F). *$p < 0.05$, **$p < 0.01$, ***$p < 0.001$, and ****$p < 0.0001$ by two-way ANOVA (A–C and E) and one-way ANOVA (D and F). ns, not significant. Data are representative of at least two independent experiments (A–F).

Tumor-intrinsic ICAM-1 is critical for immune evasion for both MHC-I-sufficient and deficient tumors

To determine the significance of ICAM-1 in anti-tumor immunity *in vivo*, we inoculated mice with ICAM-1-overexpressing cells (*Icam1*^{OE}) (Figure S2F). In both B16F10 and 4T1 models, tumors overexpressed with *Icam1* showed significantly slower growth as compared to control tumors in immune-competent mice (Figure 2A). However, both types of tumors grew at similar rates in immune-deficient NSG mice (Figure 2B), suggesting that tumor-intrinsic *Icam1* expression is important for immune-mediated control of tumor growth. Since 4T1 cells express ICAM-1 upon stimulation with IFN-γ (Figure 1D), we also generated *Icam1* KO 4T1 cells and assessed their impact on *in vivo* tumor growth (Figures S3A and S3B). Consistently, *Icam1* KO 4T1 tumors exhibited much faster growth in immune-competent mice as compared to control tumors, but the effect was abolished in NSG mice (Figure 2C). We then analyzed the number of tumor-infiltrating immune cells in *Icam1*^{OE}, *Icam1* KO, and control

tumors. The numbers of $CD45^+$ immune cells, including $CD8^+$ T cells and granzyme B+ cytotoxic T cells, were substantially decreased in *Icam1* KO 4T1 tumors compared to control tumors (Figures 2D and S3C). Consistently, these immune cells were significantly increased in *Icam1*^{OE} tumors (Figure S3D). Together, these data suggest that tumor-intrinsic ICAM-1 expression is crucial for anti-tumor immune response.

Since ICAM-1 is also crucial for NK-mediated killing, we generated *B2m*/*Icam1* double KO (dKO) 4T1 cells (Figure S3E). This allowed us to assess whether ICAM-1 expression is necessary for the immune-mediated control of MHC-I-deficient tumors, which are resistant to CTL-mediated killing but sensitive to NK-mediated killing.[23] Interestingly, even in the absence of MHC-I, the *Icam1* KO tumors showed accelerated progression compared to control tumors in immune-competent mice (Figure 2E). This phenotype was not observed in immunodeficient NSG mice (Figure 2E), indicating that the expression of ICAM-1 is also crucial for anti-tumor immunity against MHC-I-deficient tumors. Importantly, the infiltration of $CD45^+$ immune cells, including NK cells, was substantially reduced in *B2m*/*Icam1* dKO tumors compared to control tumors (Figure 2F). To assess the relevance of our findings in human cancer, we conducted an analysis of TCGA RNA-seq data. We observed a strong and positive correlation between ICAM-1 expression levels and the estimated levels of CTL and NK cell infiltration in many cancer types, such as NSCLC, thyroid carcinoma, and metastatic melanoma (Figure S3F). Taken together, these results highlight the critical role of tumor-intrinsic ICAM-1 in anti-tumor immunity.

ICAM-1 is epigenetically co-regulated with a wide range of pro-inflammatory genes in tumor cells

We next investigated the mechanism by which ICAM-1 is regulated in tumor cells. We used two complimentary approaches to elucidate the regulatory mechanisms associated with ICAM-1 expression. We first examined the genes whose expressions are co-regulated with ICAM-1. To this end, we sorted A549 cells into ICAM-1^{high} and ICAM-1^{low} populations, followed by RNA-seq and differential gene expression analysis (Figure S4A). Remarkably, ICAM-1^{high} tumors exhibited elevated expression of genes involved in type I and II interferon responses (e.g., *IRF7*, *ISG15*, *DDX58*, *IFIT1*, and *MX1*), inflammatory cytokines and chemokines (e.g., *IL6*, *CCL2*, *CCL5*, *CXCL10*, and *CXCL11*), antigen presentation pathway (e.g., *B2M*, *HLA-A*, *TAP1*, *TAP2*, and *NLRC5*), and cancer antigens (e.g., *CT83* and *MAGEA1*) (Figures S4B and S4C), suggesting that ICAM-1 is co-regulated with a pro-inflammatory gene expression program.

To identify genes and pathways that directly regulate ICAM-1 expression, we conducted a genome-wide CRISPR screen in A549 cells, in which ICAM-1 expression is low. A549-Cas9 cells were transduced with a genome-wide single-guide RNA (sgRNA) library and subsequently sorted into ICAM-1^{high} and ICAM-1^{low} populations (Figure 3A). The abundance of sgRNAs in these ICAM-1^{high} and ICAM-1^{low} groups was compared to that in unsorted control cells. To identify the positive regulators of ICAM-1, we focused on sgRNAs that were depleted in the ICAM-1^{high} population compared to control cells (Table S1). As expected, sgRNAs targeting ICAM-1 itself were the most depleted hits in this screen (Figure 3B). Interestingly, sgRNAs targeting positive regulators of the nuclear factor κB (NF-κB) pathway, such as *RELA*, *TRAF6*, and *MAP3K7*, were also significantly depleted in the ICAM-1^{high} group (Figures 3B and 3C). Conversely, sgRNAs targeting deubiquitinases known to negatively regulate NF-κB, such as *CYLD*, *TNFAIP3*, and *OTUD5*, were enriched in the ICAM-1^{high} fraction (Figures 3B and 3C). This suggests that NF-κB signaling is essential for ICAM-1 expression, which aligns with the observation that ICAM-1 is co-expressed with many pro-inflammatory genes.

Subsequently, we shifted our focus to the sgRNAs enriched in the ICAM-1^{high} group, as they likely target negative regulators of ICAM-1. Gene ontology analysis of the top 100 genes with enriched sgRNAs revealed a predominance of pathways related to histone modification and chromatin binding (Figure 3D). This suggests that ICAM-1 expression might be repressed through epigenetic mechanisms. These pathways included components of major epigenetic complexes such as DNA methylation processes (*UHRF1* and *DNMT1*), the polycomb repressive complex (PRC) 1 (*RNF2*, *RING1*, and *BMI1*), PRC 2 (*EZH2*, *SUZ12*, and *EED*), the Spt-Ada-Gcn5 acetyltransferase (SAGA) complex (*TAF5L*, *TADA1*, *TADA2B*, *MBD2*, and *TAF6L*), and the nucleosome remodeling factor (NURF) complex (*BPTF* and *SMARCA5*) (Figures 3C and S4D). To validate our screening results, we used CRISPR-Cas9 to target the components involved in DNA methylation (*UHRF1* and *DNMT1*), the PRC (*EED*), the NURF complex (*BPTF*), and cohesion regulation (*STAG2*) in A549 cells (Table S2; Figure S5A). Indeed, the loss of these genes consistently led to increased ICAM-1 expression in A549 cells (Figure 3E), supporting the idea that ICAM-1 expression is suppressed through various epigenetic mechanisms. Additionally, RNA-seq analysis reveals that alongside ICAM-1, a pro-inflammatory gene expression signature is co-upregulated upon KO of epigenetic regulators (Figures S5B and S5C). Notably, knocking out components of the DNA methylation inheritance pathway, particularly UHRF1 and DNMT1, results in the most significant upregulation of ICAM-1 and other inflammatory genes (Figures 3E and S5B and S5C).

Additionally, we also validated the role of these epigenetic regulators in SKBR3 cells (Table S2), in which ICAM-1 expression is completely silenced. Interestingly, KO of DNA methylation regulators (UHRF1 and DNMT1) led to a significant increase in ICAM-1 expression in SKBR3 cells (Figure S5D), as well as in B16F10 and 4T1 murine tumor cells (Figure S5E), confirming DNA methylation as a major silencing mechanism across different cell models. However, KO of other regulators, such as PRC and NURF components, did not induce ICAM-1 expression in SKBR3 cells (Figure S5D), suggesting that their regulation of ICAM-1 may be context dependent. These findings suggest that the DNA methylation inheritance pathway, mediated by UHRF1-DNMT1, acts as a potent inhibitor of ICAM-1 expression.

UHRF1-DNMT1-mediated methylation is a major ICAM-1 silencing mechanism in cancer cells

As UHRF1 is responsible for DNA methylation by recognizing hemi-methylated CpGs through its SET and RING-associated (SRA) domain or specific histone marks, such as H3K9me2/me3, through its tandem tudor domain (TTD),[24,25] we aimed to determine which signal and domain are responsible for the

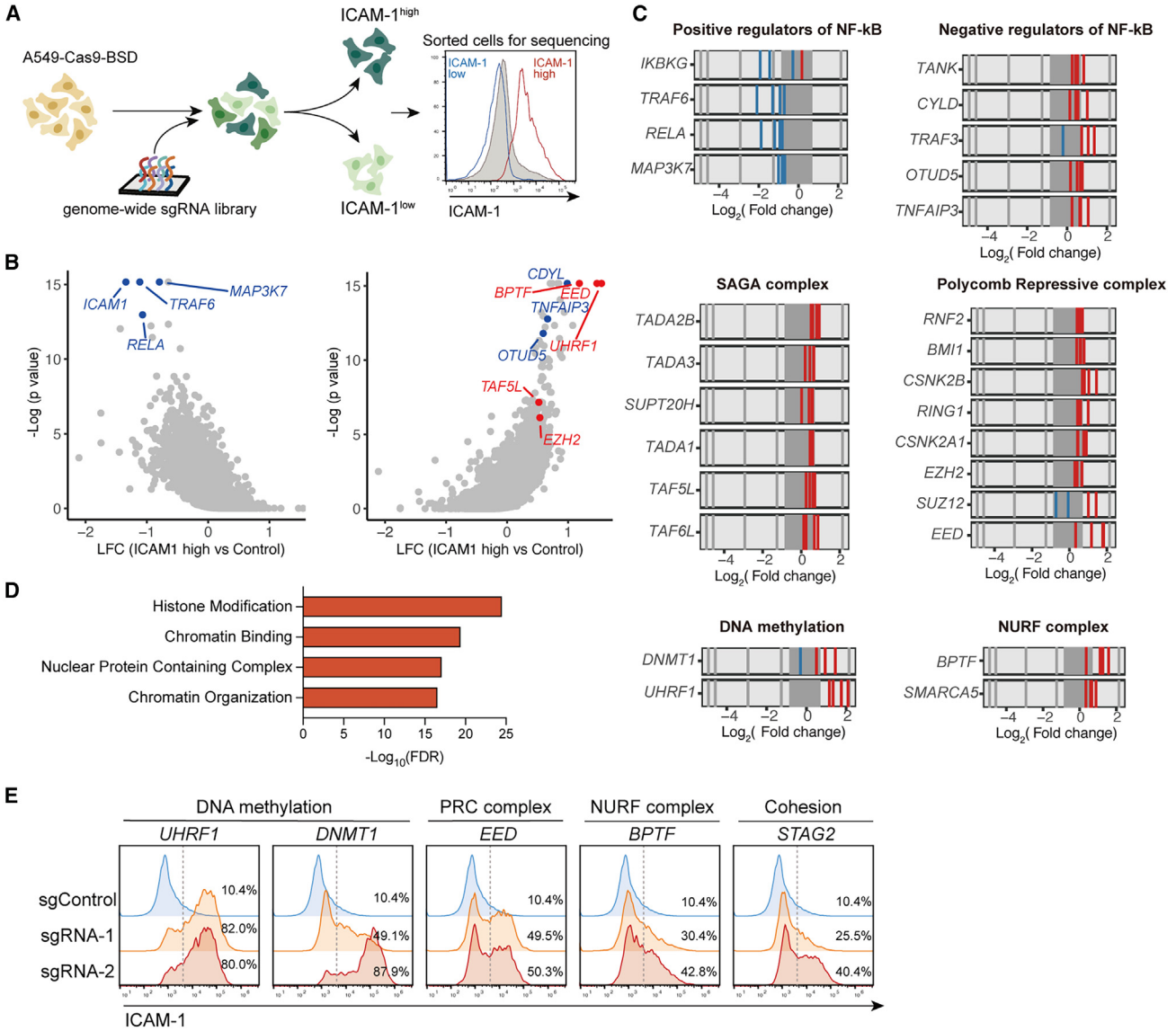

Figure 3. ICAM-1 is co-expressed with a wide range of pro-inflammatory genes and is epigenetically regulated in tumor cells

(A) Workflow of CRISPR screen to identify regulators of ICAM-1 expression. Cas9-expressing A549 cells were transduced with a genome-wide sgRNA library. CRISPR-edited A549 cells were then sorted into ICAM-1^{high} and ICAM-1^{low} fractions, followed by genomic DNA extraction and sequencing to determine the sgRNA abundance.

(B) Volcano plot showing the $\log_2$ fold change and *p* values of ICAM-1 regulators identified from CRISPR screen. The left graph shows the depleted hits (KO of the gene reduced ICAM-1 expression) and the right graph shows the enriched hits (KO of the gene enhanced ICAM-1 expression). Annotated genes represent the NF-κB pathway (blue) and epigenetic regulators (red).

(C) Log_2 fold change of sgRNAs against indicated genes in ICAM-1^{high} A549 cells as compared with control. Depleted sgRNA (KO leads to reduced ICAM-1) and enriched sgRNAs (KO leads to enhanced ICAM-1) are labeled in blue and red bars, respectively. The control sgRNAs are indicated by gray bars.

(D) Gene ontology (GO) analysis in top 100 enriched hits from ICAM-1^{high} A549 cells of CRISPR screen.

(E) FACS analysis of ICAM-1 level on A549-Cas9 cells expressing control sgRNA or sgRNAs targeting UHRF1, DNMT1, EED, BPTF, and STAG2. The same control sample was used for all comparisons shown in the panel. Data are representative of two independent experiments (E).

methylation of ICAM-1. We reconstituted UHRF1 KO cells with mutant UHRF1, in which the functions of key domains were disrupted by introducing point mutations that have been previously characterized (Figure 4A).[26–28] Our results showed that reconstitution with a dysfunctional SRA domain, the key domain for UHRF1 to maintain DNA methylation on the CpG dinucleotides during DNA replication,[24] failed to suppress ICAM-1 expression compared to wild-type UHRF1 (Figures 4B and 4C). These data suggest that UHRF1-mediated recognition of hemi-methylated CpGs is required to suppress the expression of ICAM-1.

We then performed whole-genome bisulfite sequencing (WGBS) on UHRF1 KO and control A549 cells, respectively. As

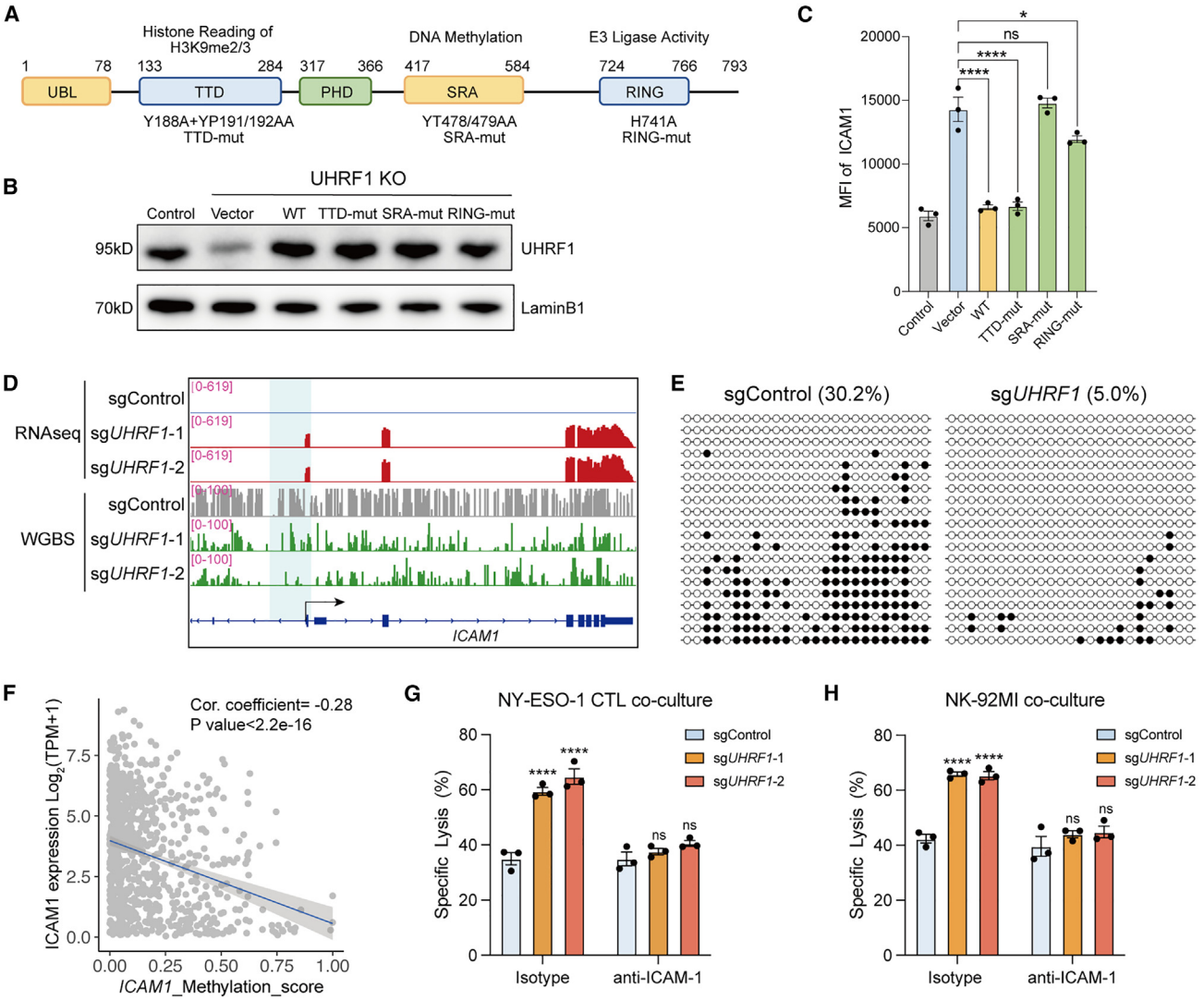

Figure 4. UHRF1-DNMT1-mediated methylation is a major ICAM-1 silencing mechanism in cancer cells

(A) Illustration of functional domains in UHRF1. The indicated point mutations abolish the corresponding functions of the domains.

(B) Western blot analysis of UHRF1 protein level in control and UHRF1 KO A549 cells expressing indicated UHRF1 mutants.

(C) Mean fluorescence intensity (MFI) of surface ICAM-1 level determined by flow cytometry in cells expressing indicated UHRF1 mutants ($n = 3$).

(D) RNA-seq and WGBS profiles of *ICAM1* in UHRF1 KO and control A549 cells. CpG region is shaded in blue. One of representative biological replicates is shown for each sample.

(E) Bisulfite sequencing of the *ICAM1* CpG region in control (left) and UHRF1 KO (right) A549 cells. Each line represents a single clone ($n = 20$). Methylated CpG sites are shown in black circles and unmethylated sites in blank circles. The percentages of overall methylated CpGs are indicated.

(F) Pearson's correlation of tumor ICAM-1 expression and *ICAM1* promoter methylation score from the CCLE database.

(G and H) Control or UHRF1 KO A549 cells co-cultured either with NY-ESO-1-specific CTLs (G) or NK-92MI cells (H) in the presence of isotype (mouse IgG1 kappa antibodies) or anti-ICAM-1-blocking antibodies (5 μg/mL). Specific lysis percentage was determined by FACS, counting the number of alive cells after co-culture with NY-ESO-1-specific CTLs or NK-92MI cells, as compared with control group ($n = 3$).

Data are presented as means ± SEM (C and G and H). $^{*}p < 0.05$ and $^{****}p < 0.0001$ by one-way ANOVA (C) and two-way ANOVA (G and H). ns, not significant. Data are representative of at least two independent experiments (B, C, G, and H).

expected, the control cells showed a normal bi-modal distribution of CpG methylation pattern, in which most of the CpGs are either in the methylated or non-methylated state (Figure S6A). In contrast, UHRF1 KO cells showed a substantial loss of fully methylated CpGs (Figure S6A), suggesting global hypomethylation. We next analyzed the differentially methylated sites between UHRF1 KO and control A549 cells. The majority of hypomethylated sites in UHRF1 KO cells were located at intergenic and intronic regions, whereas about 4% of the hypomethylated sites were located at the promoter region (Figure S6B). Notably, we found that the methylation status on the *ICAM1* CpG region (blue shade) was hypomethylated in UHRF1 KO cells as

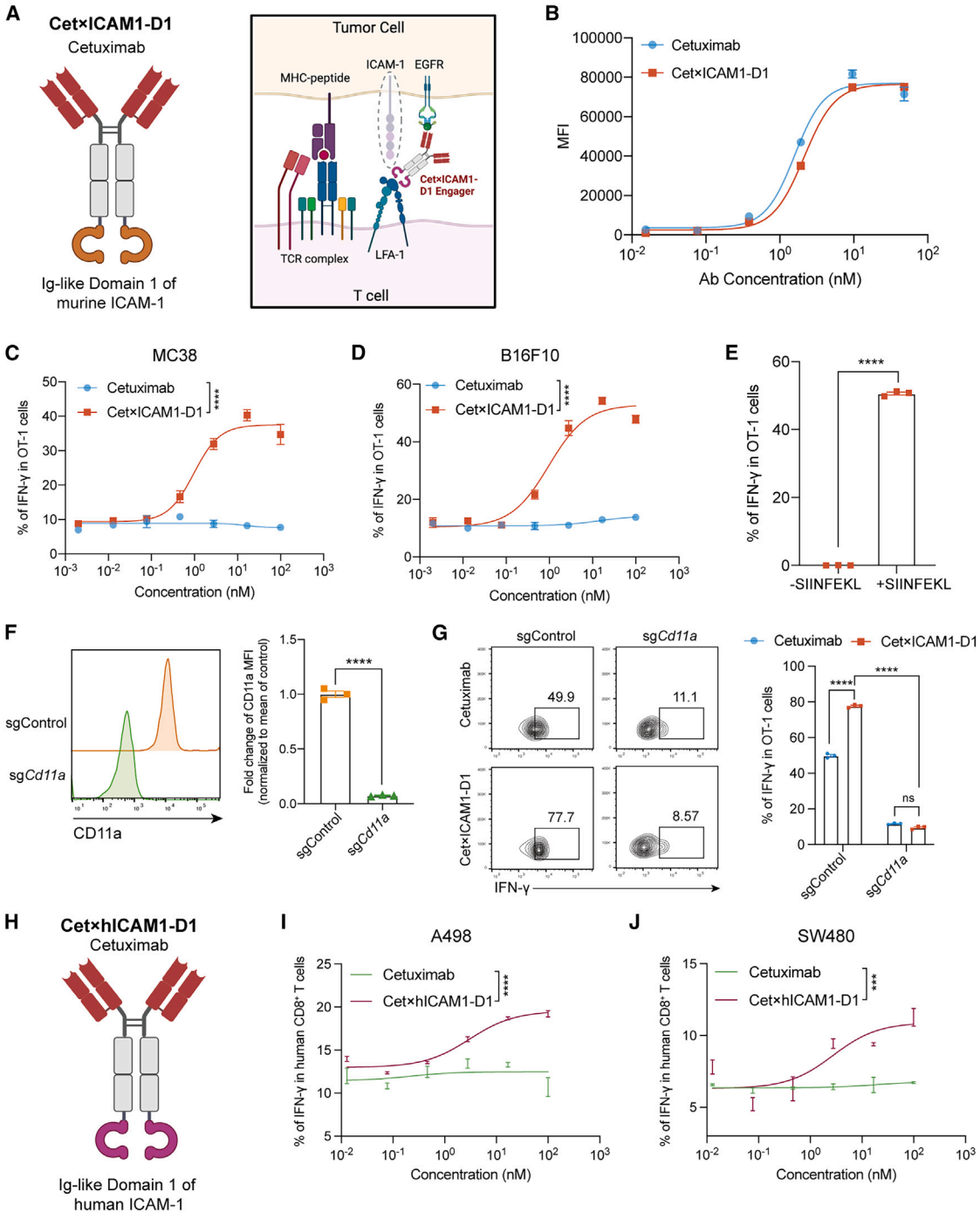

Figure 5. Reconstitution of ICAM-1/LFA-1 signaling through fusion protein Cet×ICAM1-D1

(A) Schematic structure of Cet×ICAM1-D1 fusion protein (left) and working hypothesis (right). Cet×ICAM1-D1 is composed of Fab fragment of cetuximab and murine natural D1 domain of ICAM-1, fused to a "LALA-PG" human Fc fragment. Working hypothesis: in the absence of ICAM-1, the fusion protein could interact and activate with LFA-1 signaling through the ICAM-1 D1 domain.

(B) Binding affinity of cetuximab and Cet×ICAM1-D1 to EGFR in MC38 cells (n = 3).

(C and D) OT-1 T cells were co-cultured with MC38 (C) and B16F10 (D) tumor cells with serial dilutions of Cet×ICAM1-D1 or cetuximab. FACS analysis showing the percentage of intracellular IFN-γ-producing OT-I T cells (n = 3).

(E) OT-1 cells were co-cultured with SIINFEKL-pulsed or unpulsed MC38 tumor cells in the presence of 10 nM Cet×ICAM1-D1. FACS analysis showing the percentage of intracellular IFN-γ-producing OT-I T cells (n = 3).

(legend continued on next page)

compared to controls (Figure 4D). The hypomethylation of the *ICAM1* CpG region in UHRF1 KO cells was also confirmed by bisulfite PCR analysis in both A549 and SKBR3 cells (Figures 4E and S6C). Additionally, we found that the *ICAM1* promoter methylation status also highly correlated with ICAM-1 expression in 1,086 human cancer cell lines in the CCLE database (Figure 4F). These data suggest that UHRF1-mediated DNA methylation is responsible for the silencing of ICAM-1 expression in cancer cells.

To determine whether targeting the DNA methylation pathway could enhance T and NK cell-mediated killing through ICAM-1 upregulation, we conducted *in vitro* co-culture experiments to assess the susceptibility of UHRF1-deficient A549 cells to immune cell-mediated killing. We observed that UHRF1 KO significantly increased the sensitivity of A549 cells to NY-ESO-1-specific CTL-mediated killing and NK-92MI cell-mediated killing in an ICAM-1-dependent manner, as blocking antibodies against ICAM-1 abolished the sensitive phenotype observed in the co-culture experiments (Figures 4G and 4H). In line with our genetic findings, treatment with the DNA methylation inhibitor GSK3685032,[29] which targets DNMT1, robustly induced ICAM-1 expression (Figure S6D) and enhanced the sensitivity of both A549-NY-ESO-1 and SKBR3-NY-ESO-1 cells to NY-ESO-1-specific T cell and NK92-MI-mediated killing, again in an ICAM-1-dependent manner (Figures S6E and S6F). Taken together, these data suggest that UHRF1/DNMT1-mediated DNA methylation is a major mechanism that suppresses ICAM-1 expression and its pro-killing effect in tumor cells.

Reconstitution of ICAM-1/LFA-1 signaling through fusion protein Cet×ICAM1-D1

Next, we explored therapeutic strategies for boosting T cell-mediated killing by specifically reconstituting ICAM-1/LFA-1 signaling in tumor cells in the absence of ICAM-1 expression. Previous structural studies suggest that the dimerization of the first Ig-like domain (D1) of ICAM-1 is essential for binding to LFA-1.[30] Therefore, we engineered a fusion protein, referred as Cet×ICAM1-D1, that comprises (1) Fab fragments of cetuximab (Cet) that target epidermal growth factor receptor (EGFR) as a tumor-associated antigen (TAA) and (2) a D1 domain of ICAM-1 fused to each Fc fragment (Figure 5A). This design could facilitate the potential dimerization of the D1 domain for effective LFA-1 binding (Figure S7A). Additionally, the CH2 domains of the antibodies were engineered with "LALA-PG" mutations[31] that reduce the binding to Fcγ receptor to avoid unwanted antibody-dependent cellular cytotoxicity (ADCC) or antibody-dependent cellular phagocytosis (ADCP) effect mediated by cetuximab. We first confirmed the purity and molecular weight of the fusion protein by gel electrophoresis (Figure S7B). We then engineered murine tumor cell lines MC38 and B16F10, both of which are ICAM-1 negative, to express a mutant version of chimeric murine EGFR (Figure S7C). In this mutant, six amino acids were altered to enable the binding of the anti-human EGFR antibody cetuximab,[32] while maintaining low immunogenicity to ensure successful tumor engraftment. We confirmed that Cet×ICAM1-D1 binds to the EGFR on the MC38 tumor cell line as effectively as cetuximab does (Figure 5B).

To assess the ability of Cet×ICAM1-D1 to enhance T cell-mediated cytotoxicity, we performed *in vitro* co-culture experiments, in which tumor cells were co-incubated with OT-1 cells in the presence of either bispecific Cet×ICAM1-D1 or cetuximab. In both the MC38 and B16F10 cell lines, Cet×ICAM1-D1 substantially increased IFN-γ expression when co-cultured with SIINFEKL-pulsed tumor cells—a response not observed with cetuximab (Figures 5C and 5D). Notably, IFN-γ production by T cells in response to Cet×ICAM1-D1 only occurs when tumor cells are pulsed with the SIINFEKL antigen, indicating that Cet×ICAM1-D1 functions in a signal 1 (TCR-MHC-I)-dependent manner (Figure 5E). To further confirm that the effect is specifically mediated by LFA-1 signaling on T cells, we employed CRISPR-Cas9 to knock out CD11a, which encodes a subunit of LFA-1, in OT-I T cells (Figure 5F). As expected, the KO of CD11a completely abolished the Cet×ICAM1-D1-mediated upregulation of IFN-γ expression in OT-I T cells when co-cultured with SIINFEKL-pulsed MC38 tumor cells, suggesting that Cet×ICAM1-D1 re-engages the LFA-1 signaling in T cells (Figure 5G).

We then tested the human version of fusion protein Cet×hICAM1-D1, in which the human Ig-like domain (D1) ICAM-1 is fused to cetuximab (Figure 5H). In our *in vitro* co-culture experiments, ICAM-1 KO and NY-ESO-1-positive A498 or SW480 cells with endogenous expression of EGFR were co-incubated with NY-ESO-1-specific T cells, in the presence of either Cet×hICAM1-D1 or cetuximab (Figure S7D). In both A498 and SW480 cells, the presence of Cet×hICAM1-D1 significantly enhances IFN-γ production in $CD8^+$ T cells (Figures 5I and 5J), consistent with our findings using mouse tumor cells. Together, these findings indicate that the LFA-1 engager offers a promising strategy to restore ICAM-1/LFA-1 signaling, thereby enhancing T cell-mediated cytotoxicity.

LFA-1 engager potentiates anti-tumor immunity in mouse models

We evaluated the *in vivo* therapeutic effect of Cet×ICAM1-D1 in B16F10 and MC38 mouse models by administering the treatment or a cetuximab control on day 7 post tumor inoculation, with subsequent doses every 3 days. Treatment with Cet×

(F) OT-I T cells were transduced with a control sgRNA (sgControl) or sgRNA targeting *Cd11a*. Representative FACS plot (left) and summary of mean fluorescence intensity (MFI) (right) demonstrate high knockout efficiency of *Cd11a*, as determined by CD11a staining ($n = 3$).
(G) CD11a KO or control OT-1 cells were co-cultured with MC38 tumor cells in the presence of 10 nM Cet×ICAM1-D1 or cetuximab. Representative FACS (left) and summary (right) showing the percentage of intracellular IFN-γ-producing OT1 cells in the indicated conditions ($n = 3$).
(H) Structure of the human version of the "LFA-1 engager," Cet×hICAM1-D1 fusion protein. Cet×hICAM1-D1 comprises the Fab fragment of Cetuximab and the human natural D1 domain of ICAM-1, fused to a mutant "LALA-PG" human Fc fragment.
(I and J) FACS analysis of intracellular IFN-γ production in NY-ESO-1-specific CTLs upon co-culture with A498 (I) and SW480 (J) tumor cells with serial dilutions of Cet×hICAM1-D1 or cetuximab ($n = 3$).
Data are presented as means ± SEM (B–G and I and J). ***$p < 0.001$ and ****$p < 0.0001$ by two-way ANOVA (B–D, G, and I and J) and unpaired Student's t test (E and F). ns, not significant. Data are representative of at least two independent experiments (B–G and I and J).

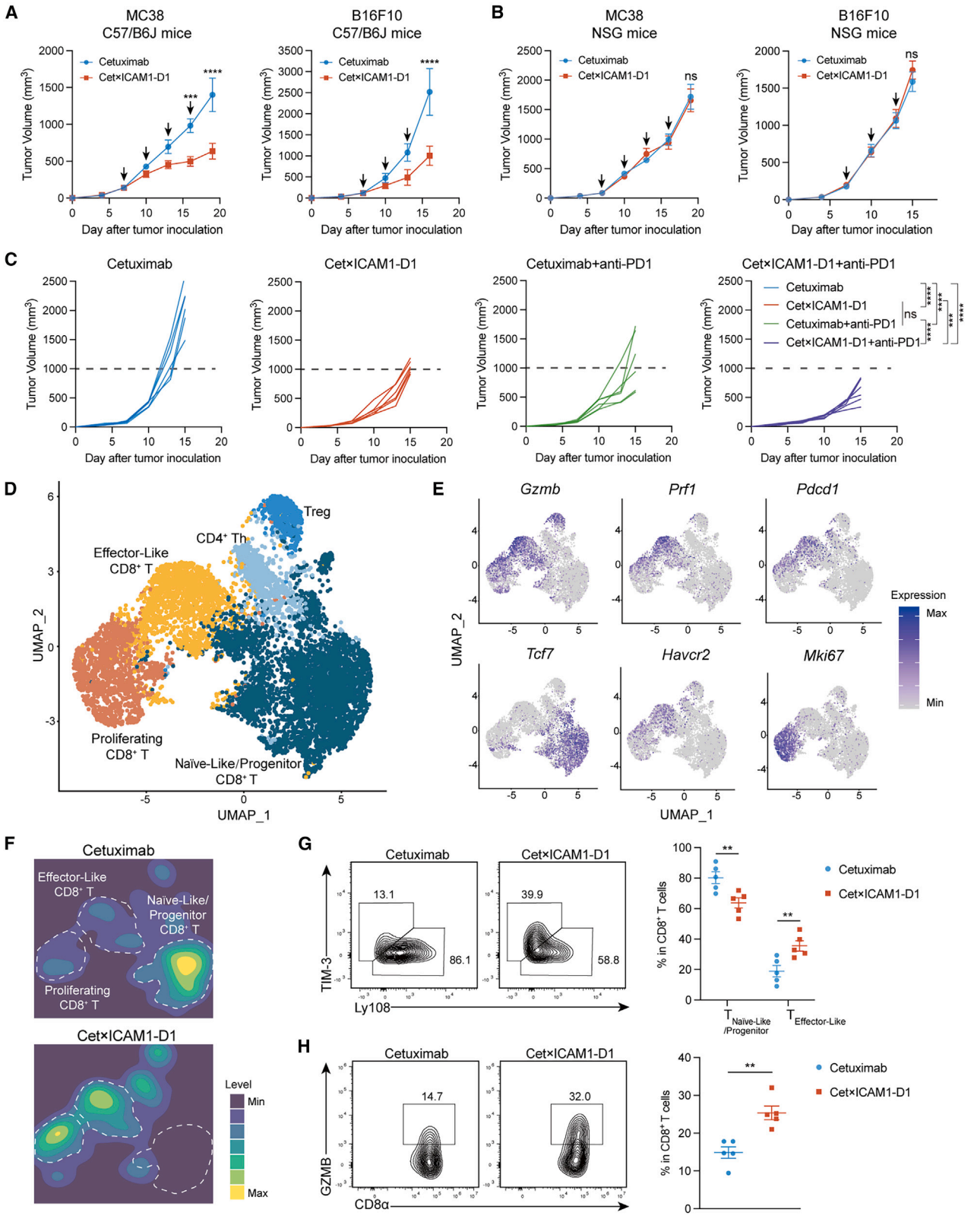

(legend on next page)

ICAM1-D1 demonstrated a substantial therapeutic effect in both models compared to the cetuximab control (Figures 6A and S7E). Both tumor types exhibited comparable growth rates in immune-deficient NSG mice under Cet×ICAM1-D1 or cetuximab treatment, indicating that the anti-tumor effects of the LFA-1 engager are immune-mediated regulation (Figure 6B). FACS analysis of tumor-infiltrating immune cells from B16F10 tumors showed that Cet×ICAM1-D1 treatment significantly increased the infiltration of immune cells ($CD45^+$), including $CD8^+$, $CD4^+$ T cells, and NK cells (Figure S7F), indicating enhanced immune cell recruitment to the tumor microenvironment. Additionally, we assessed the combined *in vivo* efficacy of Cet×ICAM1-D1 and anti-PD-1 treatment in the B16F10 model. While individual treatments with either Cet×ICAM1-D1 or anti-PD-1 showed therapeutic efficacy of the cetuximab control, the combination of Cet×ICAM1-D1 and anti-PD-1 resulted in much more substantial tumor growth inhibition and survival benefits (Figures 6C and S7G). These findings suggest a synergistic enhancement of anti-tumor immunity when Cet×ICAM1-D1 is paired with anti-PD-1 therapy.

To further characterize the potential impact of Cet×ICAM1-D1 on the tumor microenvironment, we conducted single-cell RNA-sequencing (scRNA-seq) on $CD45^+$ immune cells isolated from tumors treated with either cetuximab or Cet×ICAM1-D1 in the MC38 model. Through transcriptomic profiling, we identified $CD8^+$ T cells under different functional states, including naive-like/progenitor (*Tcf7*^{high}), proliferating (*Mki67*^{high}), and effector-like T cells (*Gzmb*^{high}; *Pdcd1*^{high}) (Figures 6D and 6E). Notably, treatment with Cet×ICAM1-D1 led to a substantial shift from naive-like/progenitor to effector-like $CD8^+$ T cells (Figures 6F and S7H), while no significant changes were observed in the myeloid compartment (Figures S8A and S8B).

To validate the scRNA-seq results, we analyzed T cell immunoglobulin domain and mucin domain-containing protein 3 (TIM-3, [*Havcr2*]) and Ly108 (*Slamf6*), a surrogate of TCF1 (*Tcf7*) expression, by flow cytometry in $CD8^+$ T cells. We observed an increased proportion of $TIM3^+Ly108^-$ effector-like and granzyme B+ $CD8^+$ T cells in the Cet×ICAM1-D1-treated tumors, alongside a decreased proportion in $TIM3^-Ly108^+$ naive-like/progenitor $CD8^+$ T cells compared to the cetuximab-treated tumors (Figures 6G and 6H), consistent with scRNA-seq analysis. Collectively, our data demonstrate that the fusion protein Cet×ICAM1-D1 enhances the activation and promotes effector function of $CD8^+$ T cells within the tumor microenvironment.

DISCUSSION

Immune evasion involves a complex interplay of various intrinsic factors within tumors. One common strategy for immune evasion revolves around the downregulation of critical genes pivotal for T cell-mediated cytotoxicity, including MHC-I molecules and antigen presentation pathways.[33] Nevertheless, genetic mutations in MHC and antigen-presenting pathways remain infrequent among patients with cancer. The scarcity of MHC-I loss-of-function mutations might be attributed to heightened NK-mediated elimination of MHC-I-deficient cells. Hence, the concurrent loss of function in pivotal pathways governing both CTLs and NK cell-mediated killing could strongly favor immune evasion. In this context, our study underscores that many human and murine tumors exhibit low or absent expression of ICAM-1, a critical molecule for immune synapse formation and immune co-stimulatory signal. Remarkably, the presence of ICAM-1 is essential for the effective elimination of these cells by both CTLs and NK cells. Our findings align with a study demonstrating that reduced ICAM-1 expression in solid tumors contributes to the inefficacy of chimeric antigen receptor T cell therapy.[34,35] Furthermore, leveraging murine models, we demonstrated that reinstating the ICAM-1 signal within tumor cells significantly enhances anti-tumor immune responses. Hence, our results indicate that the absence or reduced levels of ICAM-1 could serve as a pivotal mechanism for immune evasion.

The process of immune evasion involves multiple steps involving diverse tumor-intrinsic pathways, such as transcriptional, epigenetic, and metabolic regulations.[36–38] Through comprehensive genome-wide CRISPR screens, we demonstrated that ICAM-1 levels could be upregulated by targeting various epigenetic regulators in A549 cells, including the DNA methylation inheritance pathway, the PRC, the NURF complex, and the mammalian SAGA complex. However, in SKBR3 cells, KO of UHRF1 or DNMT1 resulted in the upregulation of ICAM-1, whereas KO of other regulators did not have a significant effect, suggesting that the DNA methylation inheritance pathway is the primary mechanism suppressing ICAM-1 expression. Given that DNA methylation is widely dysregulated in cancer cells,[39] the UHRF1-DNMT1-mediated silencing of ICAM-1 could represent a widely relevant immune evasion mechanism in human cancers. Indeed, we showed that using the DNMT1 inhibitor GSK3685032 could restore the sensitivity of tumor cells to T and NK cell-mediated killing in an ICAM-1-dependent manner. However, given the

Figure 6. Fusion protein Cet×ICAM1-D1 potentiates anti-tumor immunity in vivo

(A and B) Wild-type C57BL/6J mice (A) and NSG mice (B) were inoculated with MC38 (left) and B16F10 (right) tumor cells, respectively. The arrows indicate administrations of Cet×ICAM1-D1 or cetuximab intratumorally (5 mg/kg) to each group of mice. Tumor growth curves were recorded and shown. $n = 5–7$ mice per group.

(C) Wild-type C57BL/6J mice were inoculated with B16F10 tumor cells. Mice were treated with Cet×ICAM1-D1, cetuximab, or anti-PD-1 (5 mg/kg) on day 7, 10, and 13. Tumor growth curves were recorded and shown. $n = 6$ mice per group.

(D) Equal number of alive $CD45^+$ cells from cetuximab and Cet×ICAM1-D1-treated MC38 tumors were sorted and pooled for scRNA-seq analysis ($n = 7$ per group). Uniform manifold approximation and projection (UMAP) plot showing the distribution of different T cell subsets from scRNA-seq.

(E) UMAP feature plots showing expression of key markers in T cell subsets.

(F) Density plot showing the relative frequency of indicated T cell subsets in cetuximab and Cet×ICAM1-D1-treated MC38 tumors, respectively.

(G and H) Representative FACS plot (left) and summary of the percentage (right) of indicated T cell subsets in cetuximab and Cet×ICAM1-D1-treated MC38 tumors isolated on day 15 after tumor inoculation ($n = 5$).

Data are presented as means ± SEM (A and B and G and H). $^{**}p < 0.01$, $^{***}p < 0.001$ and $^{****}p < 0.0001$ by two-way ANOVA (A–C and G) and unpaired Student's t test (H). ns, not significant. Data are representative of at least two independent experiments (A–C and G and H).

extensive study of the DNMT1 pathway and its druggability in cancer,[40,41] our study focuses on therapeutic approaches that specifically reconstitute ICAM-1/LFA-1 signaling.

To reconstitute ICAM-1/LFA-1 signaling in ICAM-1 absent tumor cells, we developed antibody-based approaches using an LFA-1 engager. This engager comprises two modules: one targeting a TAA and another activating LFA-1 signaling. The fusion protein, Cet×ICAM1-D1, incorporates either the murine or human D1 domain of ICAM-1,[42,43] which is essential for binding to LFA-1 and provides a naturalistic engagement of LFA-1 signaling. Our data suggest that this design could effectively restore ICAM-1/LFA-1 signaling and potentiate anti-tumor immunity in mouse models. A key feature of our LFA-1 engager is its dependency on signal 1 (TCR-MHC-I) signaling for T cell activation, as the antibodies alone are insufficient to induce activation. This specificity ensures that without the presence of tumor antigen, the engager does not affect T cell killing, aligning with the dual co-stimulatory and adhesion roles of LFA-1 signaling. Additionally, the use of ICAM-1's natural D1 domain in the Cet×ICAM1-D1 construct activates LFA-1 signaling in a more physiological manner, reducing non-specific binding and potential unintended effects. This is in contrast to T cell engagers like CD3 BiTEs, which, although potent in inducing tumor lysis, can inadvertently bind TAA-expressed normal cells, leading to toxicity. Thus, our LFA-1 engager presents a promising and safer approach to potentiate anti-tumor immunity by leveraging the specificity and natural signaling pathways of immune cells.

In terms of identifying the potential target population for LFA-1 engagers, ICAM-1 expression levels in cancer subtypes need to be carefully evaluated. For instance, ICAM-1 is generally highly expressed in NSCLC but is expressed at low levels in small-cell lung cancer,[44] a subtype that responds poorly to ICB.[45] Similarly, in breast cancer, ICAM-1 is expressed at relatively high levels in TNBC but expressed at low levels in non-TNBC.[46–48] These observations underscore the need to consider specific cancer subtypes in the context of ICAM-1-mediated immune evasion and the potential clinical development of the LFA-1 engager.

Limitations of the study

While we have demonstrated that LFA-1 engagers effectively potentiate anti-tumor immunity in multiple mouse models where ICAM-1 expression is silenced, it remains unclear whether this effect can be consistently observed in tumors with high ICAM-1 expression or if the efficacy of LFA-1 engagers is restricted to tumors with low or absent ICAM-1 expression. Clarifying this distinction is critical for identifying the optimal clinical indications where LFA-1 engagers would be most effective. Furthermore, future studies should explore the design of LFA-1 engagers targeting alternative TAAs, such as human epidermal growth factor receptor 2 (HER2) or Claudin18.2, to expand their applicability across a broader range of tumor types.

RESOURCE AVAILABILITY

Lead contact

Further information and requests for resources and reagents should be directed to and will be fulfilled by the lead contact, Deng Pan (dpan@tsinghua.edu.cn).

Materials availability

Cell lines generated in this study will be provided by the lead contact under a material transfer agreement.

Data and code availability

- All datasets in this publication have been deposited in the NCBI Gene Expression Omnibus (GEO: GSE268920).
- This paper does not report original code.
- Any additional information related to this paper is available from the lead contact upon reasonable request.

ACKNOWLEDGMENTS

We thank all the members of the Pan and Zeng labs for their comments and suggestions. This work was supported by National Natural Science Foundation of China (NSFC) grant (82341026 [D.P.], 82073163 [D.P.], and 12226005 [Z.Z.]), the National Key Research and Development Program of China no. 2022YFC2505400 (D.P.), Tsinghua University Initiative Scientific Research Program (D.P.), and the Tsinghua-Peking University Center of Life Science (D.P. and Z.Z.).

AUTHOR CONTRIBUTIONS

Conceptualization, X.Z., C.L., Z.Z., and D.P.; methodology, X.Z., T.X., C.L., J.L., L.W., H.J., and Y.F.; validation, X.Z., C.L., Y. Hu, H.G., and J.L.; investigation, X.Z., C.L., Y. Hu, H.G., and J.L.; formal analysis, X.Z., C.L., Y. Hu, and H.G.; data curation, X.Z., T.X., Y. He, L.W., Z.Z., and D.P.; writing – original draft, Z.Z. and D.P.; writing – review and editing, X.Z., T.X., C.L., Y. Hu, and D.P.; funding acquisition, Z.Z. and D.P.; supervision, Z.Z. and D.P.

DECLARATION OF INTERESTS

Tsinghua University has filed a PCT patent related to this work, on which X.Z. and D.P. are inventors. D.P. received sponsored research funding from Bayer AG and Boehringer Ingelheim. These grants were not related to the research reported in this study.

STAR★METHODS

Detailed methods are provided in the online version of this paper and include the following:

- KEY RESOURCES TABLE
- EXPERIMENTAL MODEL AND STUDY PARTICIPANT DETAILS
  - Cell lines
  - Primary cultures
  - Mice
- METHOD DETAILS
  - Generation of cell lines
  - FACS-based genome wide CRISPR screen
  - *In vitro* tumor with NY-ESO-1 specific CTLs or NK-92MI cells co-culture
  - Cell proliferation assay
  - Western blot
  - Tracking of Indels by DEcomposition (TIDE) analysis for gene editing efficiency
  - Whole genome bisulfite sequencing (WGBS) and focused bisulfite sequencing of *ICAM1* promoter region
  - *In vivo* animal studies xenograft mouse models
  - Flow cytometry and analysis of tumor infiltrating lymphocytes
  - Bulk RNA-seq
  - Single cell RNA-seq of immune cells isolated from Cetuximab and Cet×ICAM1-D1 treated tumors
  - Single cell RNA-seq analysis
  - Analysis of ICB cohorts
  - Experiments related to fusion protein
- QUANTIFICATION AND STATISTICAL ANALYSIS

SUPPLEMENTAL INFORMATION

Supplementary data related to this article can be found online at https://doi.org/10.1016/j.xcrm.2025.101975.

Received: August 14, 2024
Revised: November 22, 2024
Accepted: January 28, 2025
Published: February 24, 2025

REFERENCES

1. Patel, S.J., Sanjana, N.E., Kishton, R.J., Eidizadeh, A., Vodnala, S.K., Cam, M., Gartner, J.J., Jia, L., Steinberg, S.M., Yamamoto, T.N., et al. (2017). Identification of essential genes for cancer immunotherapy. Nature *548*, 537–542. https://doi.org/10.1038/nature23477.
2. Pan, D., Kobayashi, A., Jiang, P., Ferrari de Andrade, L., Tay, R.E., Luoma, A.M., Tsoucas, D., Qiu, X., Lim, K., Rao, P., et al. (2018). A major chromatin regulator determines resistance of tumor cells to T cell–mediated killing. Science *359*, 770–775. https://doi.org/10.1126/science.aao1710.
3. Pech, M.F., Fong, L.E., Villalta, J.E., Chan, L.J., Kharbanda, S., O'Brien, J.J., McAllister, F.E., Firestone, A.J., Jan, C.H., and Settleman, J. (2019). Systematic identification of cancer cell vulnerabilities to natural killer cell-mediated immune surveillance. Elife *8*, e47362. https://doi.org/10.7554/eLife.47362.
4. Shimasaki, N., Jain, A., and Campana, D. (2020). NK cells for cancer immunotherapy. Nat. Rev. Drug Discov. *19*, 200–218. https://doi.org/10.1038/s41573-019-0052-1.
5. Zaretsky, J.M., Garcia-Diaz, A., Shin, D.S., Escuin-Ordinas, H., Hugo, W., Hu-Lieskovan, S., Torrejon, D.Y., Abril-Rodriguez, G., Sandoval, S., Barthly, L., et al. (2016). Mutations Associated with Acquired Resistance to PD-1 Blockade in Melanoma. N. Engl. J. Med. *375*, 819–829. https://doi.org/10.1056/nejmoa1604958.
6. Lee, J.H., Shklovskaya, E., Lim, S.Y., Carlino, M.S., Menzies, A.M., Stewart, A., Pedersen, B., Irvine, M., Alavi, S., Yang, J.Y.H., et al. (2020). Transcriptional downregulation of MHC class I and melanoma de- differentiation in resistance to PD-1 inhibition. Nat. Commun. *11*, 1897. https://doi.org/10.1038/s41467-020-15726-7.
7. Burr, M.L., Sparbier, C.E., Chan, Y.-C., Williamson, J.C., Woods, K., Beavis, P.A., Lam, E.Y.N., Henderson, M.A., Bell, C.C., Stolzenburg, S., et al. (2017). CMTM6 maintains the expression of PD-L1 and regulates anti-tumour immunity. Nature *549*, 101–105. https://doi.org/10.1038/nature23643.
8. Mezzadra, R., Sun, C., Jae, L.T., Gomez-Eerland, R., de Vries, E., Wu, W., Logtenberg, M.E.W., Slagter, M., Rozeman, E.A., Hofland, I., et al. (2017). Identification of CMTM6 and CMTM4 as PD-L1 protein regulators. Nature *549*, 106–110. https://doi.org/10.1038/nature23669.
9. Jiang, P., Gu, S., Pan, D., Fu, J., Sahu, A., Hu, X., Li, Z., Traugh, N., Bu, X., Li, B., et al. (2018). Signatures of T cell dysfunction and exclusion predict cancer immunotherapy response. Nat. Med. *24*, 1550–1558. https://doi.org/10.1038/s41591-018-0136-1.
10. Ferrari de Andrade, L., Tay, R.E., Pan, D., Luoma, A.M., Ito, Y., Badrinath, S., Tsoucas, D., Franz, B., May, K.F., Harvey, C.J., et al. (2018). Antibody-mediated inhibition of MICA and MICB shedding promotes NK cell–driven tumor immunity. Science *359*, 1537–1542. https://doi.org/10.1126/science.aao0505.
11. Tauriello, D.V.F., Sancho, E., and Batlle, E. (2022). Overcoming TGFβ-mediated immune evasion in cancer. Nat. Rev. Cancer *22*, 25–44. https://doi.org/10.1038/s41568-021-00413-6.
12. Grakoui, A., Bromley, S.K., Sumen, C., Davis, M.M., Shaw, A.S., Allen, P.M., and Dustin, M.L. (1999). The Immunological Synapse: A Molecular Machine Controlling T Cell Activation. Science *285*, 221–227. https://doi.org/10.1126/science.285.5425.221.
13. Huppa, J.B., and Davis, M.M. (2003). T-cell-antigen recognition and the immunological synapse. Nat. Rev. Immunol. *3*, 973–983. https://doi.org/10.1038/nri1245.
14. Xie, J., Tato, C.M., and Davis, M.M. (2013). How the immune system talks to itself: the varied role of synapses. Immunol. Rev. *251*, 65–79. https://doi.org/10.1111/imr.12017.
15. Sligh, J.E., Ballantyne, C.M., Rich, S.S., Hawkins, H.K., Smith, C.W., Bradley, A., and Beaudet, A.L. (1993). Inflammatory and immune responses are impaired in mice deficient in intercellular adhesion molecule 1. Proc. Natl. Acad. Sci. USA *90*, 8529–8533. https://doi.org/10.1073/pnas.90.18.8529.
16. Ma, V.P.-Y., Hu, Y., Kellner, A.V., Brockman, J.M., Velusamy, A., Blanchard, A.T., Evavold, B.D., Alon, R., and Salaita, K. (2022). The magnitude of LFA-1/ICAM-1 forces fine-tune TCR-triggered T cell activation. Sci. Adv. *8*, eabg4485. https://doi.org/10.1126/sciadv.abg4485.
17. Chen, S., Zhang, S., Chen, S., and Ma, F. (2023). The prognostic value and immunological role of CD44 in pan-cancer study. Sci. Rep. *13*, 7011. https://doi.org/10.1038/s41598-023-34154-3.
18. Munz, M., Baeuerle, P.A., and Gires, O. (2009). The Emerging Role of EpCAM in Cancer and Stem Cell Signaling. Cancer Res. *69*, 5627–5629. https://doi.org/10.1158/0008-5472.CAN-09-0654.
19. Gires, O., Pan, M., Schinke, H., Canis, M., and Baeuerle, P.A. (2020). Expression and function of epithelial cell adhesion molecule EpCAM: where are we after 40 years? Cancer Metastasis Rev. *39*, 969–987. https://doi.org/10.1007/s10555-020-09898-3.
20. Hwang, S., Kwon, A.-Y., Jeong, J.-Y., Kim, S., Kang, H., Park, J., Kim, J.-H., Han, O.J., Lim, S.M., and An, H.J. (2020). Immune gene signatures for predicting durable clinical benefit of anti-PD-1 immunotherapy in patients with non-small cell lung cancer. Sci. Rep. *10*, 643. https://doi.org/10.1038/s41598-019-57218-9.
21. Kim, S.T., Cristescu, R., Bass, A.J., Kim, K.-M., Odegaard, J.I., Kim, K., Liu, X.Q., Sher, X., Jung, H., Lee, M., et al. (2018). Comprehensive molecular characterization of clinical responses to PD-1 inhibition in metastatic gastric cancer. Nat. Med. *24*, 1449–1458. https://doi.org/10.1038/s41591-018-0101-z.
22. Miao, D., Margolis, C.A., Gao, W., Voss, M.H., Li, W., Martini, D.J., Norton, C., Bossé, D., Wankowicz, S.M., Cullen, D., et al. (2018). Genomic correlates of response to immune checkpoint therapies in clear cell renal cell carcinoma. Science *359*, 801–806. https://doi.org/10.1126/science.aan5951.
23. Guillerey, C., Huntington, N.D., and Smyth, M.J. (2016). Targeting natural killer cells in cancer immunotherapy. Nat. Immunol. *17*, 1025–1036. https://doi.org/10.1038/ni.3518.
24. Bostick, M., Kim, J.K., Estève, P.-O., Clark, A., Pradhan, S., and Jacobsen, S.E. (2007). UHRF1 Plays a Role in Maintaining DNA Methylation in Mammalian Cells. Science *317*, 1760–1764. https://doi.org/10.1126/science.1147939.
25. Fang, J., Cheng, J., Wang, J., Zhang, Q., Liu, M., Gong, R., Wang, P., Zhang, X., Feng, Y., Lan, W., et al. (2016). Hemi-methylated DNA opens a closed conformation of UHRF1 to facilitate its histone recognition. Nat. Commun. *7*, 11197. https://doi.org/10.1038/ncomms11197.
26. Liu, X., Gao, Q., Li, P., Zhao, Q., Zhang, J., Li, J., Koseki, H., and Wong, J. (2013). UHRF1 targets DNMT1 for DNA methylation through cooperative binding of hemi-methylated DNA and methylated H3K9. Nat. Commun. *4*, 1563. https://doi.org/10.1038/ncomms2562.
27. Harrison, J.S., Cornett, E.M., Goldfarb, D., DaRosa, P.A., Li, Z.M., Yan, F., Dickson, B.M., Guo, A.H., Cantu, D.V., Kaustov, L., et al. (2016). Hemi-methylated DNA regulates DNA methylation inheritance through allosteric activation of H3 ubiquitylation by UHRF1. Elife *5*, e17101. https://doi.org/10.7554/eLife.17101.
28. Kong, X., Chen, J., Xie, W., Brown, S.M., Cai, Y., Wu, K., Fan, D., Nie, Y., Yegnasubramanian, S., Tiedemann, R.L., et al. (2019). Defining UHRF1 Domains that Support Maintenance of Human Colon Cancer DNA

Methylation and Oncogenic Properties. Cancer Cell *35*, 633–648.e7. https://doi.org/10.1016/j.ccell.2019.03.003.

29. Pappalardi, M.B., Keenan, K., Cockerill, M., Kellner, W.A., Stowell, A., Sherk, C., Wong, K., Pathuri, S., Briand, J., Steidel, M., et al. (2021). Discovery of a first-in-class reversible DNMT1-selective inhibitor with improved tolerability and efficacy in acute myeloid leukemia. Nat. Cancer *2*, 1002–1017. https://doi.org/10.1038/s43018-021-00249-x.
30. Jun, C.-D., Shimaoka, M., Carman, C.V., Takagi, J., and Springer, T.A. (2001). Dimerization and the effectiveness of ICAM-1 in mediating LFA-1-dependent adhesion. Proc. Natl. Acad. Sci. USA *98*, 6830–6835. https://doi.org/10.1073/pnas.121186998.
31. Saunders, K.O. (2019). Conceptual Approaches to Modulating Antibody Effector Functions and Circulation Half-Life. Front. Immunol. *10*, 1296. https://doi.org/10.3389/fimmu.2019.01296.
32. Liu, L., Chen, J., Bae, J., Li, H., Sun, Z., Moore, C., Hsu, E., Han, C., Qiao, J., and Fu, Y.-X. (2021). Rejuvenation of tumour-specific T cells through bispecific antibodies targeting PD-L1 on dendritic cells. Nat. Biomed. Eng. *5*, 1261–1273. https://doi.org/10.1038/s41551-021-00800-2.
33. Jhunjhunwala, S., Hammer, C., and Delamarre, L. (2021). Antigen presentation in cancer: insights into tumour immunogenicity and immune evasion. Nat. Rev. Cancer *21*, 298–312. https://doi.org/10.1038/s41568-021-00339-z.
34. Kantari-Mimoun, C., Barrin, S., Vimeux, L., Haghiri, S., Gervais, C., Joaquina, S., Mittelstaet, J., Mockel-Tenbrinck, N., Kinkhabwala, A., Damotte, D., et al. (2021). CAR T-cell Entry into Tumor Islets Is a Two-Step Process Dependent on IFNγ and ICAM-1. Cancer Immunol. Res. *9*, 1425–1438. https://doi.org/10.1158/2326-6066.CIR-20-0837.
35. Larson, R.C., Kann, M.C., Bailey, S.R., Haradhvala, N.J., Llopis, P.M., Bouffard, A.A., Scarfó, I., Leick, M.B., Grauwet, K., Berger, T.R., et al. (2022). CAR T cell killing requires the IFNγR pathway in solid but not liquid tumours. Nature *604*, 563–570. https://doi.org/10.1038/s41586-022-04585-5.
36. Spranger, S., and Gajewski, T.F. (2018). Mechanisms of Tumor Cell–Intrinsic Immune Evasion. Annu. Rev. Cancer Biol. *2*, 213–228. https://doi.org/10.1146/annurev-cancerbio-030617-050606.
37. Wellenstein, M.D., and De Visser, K.E. (2018). Cancer-Cell-Intrinsic Mechanisms Shaping the Tumor Immune Landscape. Immunity *48*, 399–416. https://doi.org/10.1016/j.immuni.2018.03.004.
38. Cao, J., and Yan, Q. (2020). Cancer Epigenetics, Tumor Immunity, and Immunotherapy. Trends Cancer *6*, 580–592. https://doi.org/10.1016/j.trecan.2020.02.003.
39. Nishiyama, A., and Nakanishi, M. (2021). Navigating the DNA methylation landscape of cancer. Trends Genet. *37*, 1012–1027. https://doi.org/10.1016/j.tig.2021.05.002.
40. Yoo, C.B., and Jones, P.A. (2006). Epigenetic therapy of cancer: past, present and future. Nat. Rev. Drug Discov. *5*, 37–50. https://doi.org/10.1038/nrd1930.
41. Bates, S.E. (2020). Epigenetic Therapies for Cancer. N. Engl. J. Med. *383*, 650–663. https://doi.org/10.1056/NEJMra1805035.
42. Staunton, D.E., Dustin, M.L., Erickson, H.P., and Springer, T.A. (1990). The arrangement of the immunoglobulin-like domains of ICAM-1 and the binding sites for LFA-1 and rhinovirus. Cell *61*, 243–254. https://doi.org/10.1016/0092-8674(90)90805-O.
43. Shimaoka, M., Xiao, T., Liu, J.-H., Yang, Y., Dong, Y., Jun, C.-D., McCormack, A., Zhang, R., Joachimiak, A., Takagi, J., et al. (2003). Structures of the αL I Domain and Its Complex with ICAM-1 Reveal a Shape-Shifting Pathway for Integrin Regulation. Cell *112*, 99–111. https://doi.org/10.1016/S0092-8674(02)01257-6.
44. Schardt, C., Heymanns, J., Schardt, C., Rotsch, M., and Havemann, K. (1993). Differential expression of the intercellular adhesion molecule-1 (ICAM-1) in lung cancer cell lines of various histological types. Eur. J. Cancer *29*, 2250–2255. https://doi.org/10.1016/0959-8049(93)90217-4.
45. Konen, J.M., Wu, H., and Gibbons, D.L. (2024). Immune checkpoint blockade resistance in lung cancer: emerging mechanisms and therapeutic opportunities. Trends Pharmacol. Sci. *45*, 520–536. https://doi.org/10.1016/j.tips.2024.04.006.
46. Guo, P., Huang, J., Wang, L., Jia, D., Yang, J., Dillon, D.A., Zurakowski, D., Mao, H., Moses, M.A., and Auguste, D.T. (2014). ICAM-1 as a molecular target for triple negative breast cancer. Proc. Natl. Acad. Sci. USA *111*, 14710–14715. https://doi.org/10.1073/pnas.1408556111.
47. Figenschau, S.L., Knutsen, E., Urbarova, I., Fenton, C., Elston, B., Perander, M., Mortensen, E.S., and Fenton, K.A. (2018). ICAM1 expression is induced by proinflammatory cytokines and associated with TLS formation in aggressive breast cancer subtypes. Sci. Rep. *8*, 11720. https://doi.org/10.1038/s41598-018-29604-2.
48. Wei, H., Wang, Z., Kuang, Y., Wu, Z., Zhao, S., Zhang, Z., Li, H., Zheng, M., Zhang, N., Long, C., et al. (2020). Intercellular Adhesion Molecule-1 as Target for CAR-T-Cell Therapy of Triple-Negative Breast Cancer. Front. Immunol. *11*, 573823. https://doi.org/10.3389/fimmu.2020.573823.
49. Dobin, A., Davis, C.A., Schlesinger, F., Drenkow, J., Zaleski, C., Jha, S., Batut, P., Chaisson, M., and Gingeras, T.R. (2013). STAR: ultrafast universal RNA-seq aligner. Bioinformatics *29*, 15–21. https://doi.org/10.1093/bioinformatics/bts635.
50. Akalin, A., Kormaksson, M., Li, S., Garrett-Bakelman, F.E., Figueroa, M.E., Melnick, A., and Mason, C.E. (2012). methylKit: a comprehensive R package for the analysis of genome-wide DNA methylation profiles. Genome Biol. *13*, R87. https://doi.org/10.1186/gb-2012-13-10-r87.
51. Hao, Y., Stuart, T., Kowalski, M.H., Choudhary, S., Hoffman, P., Hartman, A., Srivastava, A., Molla, G., Madad, S., Fernandez-Granda, C., and Satija, R. (2024). Dictionary learning for integrative, multimodal and scalable single-cell analysis. Nat. Biotechnol. *42*, 293–304. https://doi.org/10.1038/s41587-023-01767-y.
52. Li, W., Xu, H., Xiao, T., Cong, L., Love, M.I., Zhang, F., Irizarry, R.A., Liu, J.S., Brown, M., and Liu, X.S. (2014). MAGeCK enables robust identification of essential genes from genome-scale CRISPR/Cas9 knockout screens. Genome Biol. *15*, 554. https://doi.org/10.1186/s13059-014-0554-4.
53. Brinkman, E.K., Chen, T., Amendola, M., and van Steensel, B. (2014). Easy quantitative assessment of genome editing by sequence trace decomposition. Nucleic Acids Res. *42*, e168. https://doi.org/10.1093/nar/gku936.
54. Kumaki, Y., Oda, M., and Okano, M. (2008). QUMA: quantification tool for methylation analysis. Nucleic Acids Res. *36*, W170–W175. https://doi.org/10.1093/nar/gkn294.
55. Abramson, J., Adler, J., Dunger, J., Evans, R., Green, T., Pritzel, A., Ronneberger, O., Willmore, L., Ballard, A.J., Bambrick, J., et al. (2024). Accurate structure prediction of biomolecular interactions with AlphaFold 3. Nature *630*, 493–500. https://doi.org/10.1038/s41586-024-07487-w.

STAR★METHODS

KEY RESOURCES TABLE

REAGENT or RESOURCE	SOURCE	IDENTIFIER
Antibodies		
anti-human-CD3	Biolegend	Cat# 317315, RRID: AB_1877070
anti-human-CD28	BD	Cat# 555725, RRID: AB_396068
InVivoPlus anti-mouse-CD3ε	Bio X Cell	Cat# BE0015-1, RRID: AB_1107624
InVivoMab anti-mouse-CD28	Bio X Cell	Cat# BE0015-1, RRID: AB_1107624
InVivoPlus anti-mouse-PD-1 (CD279)	Bio X Cell	Cat# BE0273, RRID: AB_2687796
Isotype control mouse IgG1 kappa Antibody	BioLegend	Cat# 401402, RRID: AB_2801451
Anti-ICAM1 monoclonal Antibody	Thermo Fisher Scientific	Cat# MA5407, RRID: AB_223596
APC anti-human-CD54 Antibody	BioLegend	Cat# 353112, RRID: AB_10916103
Human TruStain FcX™	BioLegend	Cat# 422302, RRID: AB_2818986
APC anti-human-CD8a Antibody	BioLegend	Cat# 301014, RRID: AB_314132
APC anti-human-CD56 Antibody	BioLegend	Cat# 318309, RRID: AB_604098
APC anti-human-IFN-γ Antibody	BioLegend	Cat# 502511, RRID: AB_315236
FITC anti-human-CD107a Antibody	BioLegend	Cat# 328605, RRID: AB_1186058
eFluor™ 450, CD44 Monoclonal Antibody (IM7) Antibody	Thermo Fisher Scientific	Cat# 48-0441-82, RRID: AB_1272246
APC anti-human-CD326 (Ep-CAM) Antibody	BioLegend	Cat# 369810, RRID: AB_2650907
APC anti-human-EGFR Antibody	BioLegend	Cat# 352905, RRID: AB_11148943
APC anti-human IgG Fc Antibody	BioLegend	Cat# 410712, RRID: AB_2565790
anti-mouse-CD16/32 Antibody	BioLegend	Cat# 101320, RRID: AB_1574975
APC anti-mouse-CD54 Antibody	BioLegend	Cat# 116119, RRID: AB_10613645
APC anti-mouse-H2Kd Antibody	BioLegend	Cat# 116619, RRID: AB_10640118
APC anti-mouse-H2Kb Antibody	BioLegend	Cat# 114614, RRID: AB_2750194
APC anti-mouse-CD11a Antibody	BioLegend	Cat# 153109, RRID: AB_2716218
Brilliant Violet 421 anti-mouse-CD45 Antibody	BioLegend	Cat# 103133, RRID: AB_10899570
FITC anti-mouse-CD3 Antibody	BioLegend	Cat# 100204, RRID: AB_312661
PE anti-mouse-CD8a Antibody	BioLegend	Cat# 100708, RRID: AB_312747
PerCP/Cyanine5.5 anti-mouse-CD8a Antibody	BioLegend	Cat# 100734, RRID: AB_2075238
Brilliant Violet 510^{C} anti-mouse-CD4 Antibody	BioLegend	Cat# 100559, RRID: AB_2562608
PerCP-eFluor™ 710-CD335 (NKp46) Monoclonal Antibody (29A1.4)	Thermo Fisher Scientific	Cat# 46-3351-80, RRID: AB_1834442
PE/Cyanine7 anti-human/mouse-Granzyme B Recombinant Antibody	BioLegend	Cat# 372214, RRID: AB_2728381
APC anti-human/mouse-Granzyme B Recombinant Antibody	BioLegend	Cat# 372203, RRID: AB_2687027
FITC anti-mouse-CD62L Antibody	BioLegend	Cat# 161211, RRID: AB_2941440
BV421 Hamster Anti-Mouse-CD279	BD	Cat# 562584, RRID: AB_2737668
PE-Cyanine7, CD366 (TIM3) Monoclonal Antibody (RMT3-23)	Thermo Fisher Scientific	Cat# 25-5870-82, RRID: AB_2573483
APC, Ly-108 Monoclonal Antibody (eBio13G3-19D (13G3-19D))	Thermo Fisher Scientific	Cat# 17-1508-82, RRID: AB_10717668
HA-Tag (C29F4) Rabbit mAb	Cell Signaling Technology	Cat# 3724, RRID: AB_1549585
Alexa Fluor 488 Conjugate anti-rabbit IgG (H + L), F(ab')2 Fragment Antibody	Cell Signaling Technology	Cat# 4412, RRID: AB_1904025
UHRF1 (D6G8E) Rabbit mAb	Cell Signaling Technology	Cat# 12387, RRID: AB_2715501

(*Continued on next page*)

Continued

REAGENT or RESOURCE	SOURCE	IDENTIFIER
Lamin B1 (D9V6H) Rabbit mAb	Cell Signaling Technology	Cat# 13435, RRID: AB_2737428
Goat Anti-Rabbit IgG (H&L)-HRP Conjugated	Easybio	Cat# BE0101-100
Bacterial and virus strains		
Stbl3 Competent Cell	AlpaLife	Cat# KTSM110
Chemicals, peptides, and recombinant proteins		
Dulbecco's Modified Eagle Medium (DMEM) basic (1X)	Thermo Fisher Scientific	Cat# C11995500BT
Roswell Park Memorial Institute (RPMI) 1640 basic (1X)	Thermo Fisher Scientific	Cat# C11875500BT
RPMI Medium 1640 (1X)	Thermo Fisher Scientific	Cat# 11875-093
McCoy's 5A Medium (Modified) (1X)	Thermo Fisher Scientific	Cat# 16600082
FreeStyle™ 293 Expression Medium	Thermo Fisher Scientific	Cat# 12338018
Opti-MEM	Thermo Fisher Scientific	Cat# 11058021
Alpha MEM without ribonucleosides	Thermo Fisher Scientific	Cat# 12000063
Sodium Bicarbonate	Sigma-Aldrich	Cat# S5761
Myo-inositol	Sigma-Aldrich	Cat# I7508
Folic acid	Sigma-Aldrich	Cat# F8758
SMM 293-TII	Sino Biological	Cat# M293TII
PBS, pH 7.4	Thermo Fisher Scientific	Cat# 10010049
Trypsin-EDTA (0.25%), phenol red	Thermo Fisher Scientific	Cat# 25200072
Penicillin-Streptomycin	Thermo Fisher Scientific	Cat# 10378016
L-Glutamine (200mM)	Thermo Fisher Scientific	Cat# 25030081
Sodium Pyruvate (100 mM)	Thermo Fisher Scientific	Cat# 11360070
MEM Non-Essential Amino Acids Solution (100x)	Thermo Fisher Scientific	Cat# 11140050
HEPES (1M)	Thermo Fisher Scientific	Cat# 15630130
2-Mercaptoethano	Thermo Fisher Scientific	Cat# 21985023
Fetal Bovine Serum (FBS)	Thermo Fisher Scientific	Cat# A5669701
Horse serum	Thermo Fisher Scientific	Cat# 26050-070
Human Fibronectin	BD	Cat# 354008
Recombinant Human IL-2 (carrier-free)	R&D system	Cat# 10453-IL
Recombinant Mouse IL-2 (carrier-free)	Biolegend	Cat# 575406
Recombinant Mouse IFN-γ (carrier-free)	Biolegend	Cat# 575306
Blasticidin	InvivoGen	Cat# ant-bl-1
Puromycin	InvivoGen	Cat# ant-pr-1
hygromycin B	InvivoGen	Cat# ant-hg-1
SIINFEKL/OVA Peptide (257–264)	GenScript	Cat# RP10611
Dimethyl Sulfoxide (DMSO)	Sigma Aldrich	Cat# D2650
GSK3685032	MCE	Cat# HY-139664
Collagenase type IV	Sigma Aldrich	Cat# C5138
DNAse type IV	Sigma Aldrich	Cat# D5025
Hyaluronidase type V	Sigma Aldrich	Cat# H6254
Cell Lysis Buffer (10X)	Cell Signaling Technology	Cat# 9803S
ACK Lysis Buffer	LEAGENE	Cat# CS0001
DAPI	Cell Signaling Technology	Cat# 4083
Fixable Viability Dye eFluor™ 506	Thermo Fisher Scientific	Cat# 65-0866-18
Brefeldin A Solution (1,000X)	Biolegend	Cat# 420601
EDTA-free Protease Inhibitor Cocktail	Sigma Aldrich	Cat# 11873580001

(*Continued on next page*)

Continued

REAGENT or RESOURCE	SOURCE	IDENTIFIER
SurePAGE, Bis-Tris, 10x8, 4–12%, 15 wells	GenScript	Cat# M00654
Tris-MOPS-SDS Running Buffer Powder	GenScript	Cat# M00138
PageRuler Prestained Protein Ladder	Thermo Fisher Scientific	Cat# 26616
Tris-buffered saline with 0.1% Tween 20 detergent (TBST)	Beyotime	Cat# ST673
Skim Milk powder	BD	Cat# 232100
SuperSignal™ West Pico PLUS Chemiluminescent Substrate	Thermo Fisher Scientific	Cat# 34580
TRIzol	Thermo Fisher Scientific	Cat# 15596026
Critical commercial assays		
EasySep™ Human CD8+ T cell Enrichment Isolation Kit	STEMCELL	Cat# 19053
MojoSort Mouse CD8 T cell Isolation Kit	Biolegend	Cat# 480007
NucleoSpin Blood XL, Maxi kit for DNA from blood	MACHEREY-NAGEL	Cat# 740954.20
NucleoSpin Tissue, Mini kit for DNA from cells and tissue	MACHEREY-NAGEL	Cat# 740952.50
NucleoSpin Gel and PCR Clean-up	MACHEREY-NAGEL	Cat# 740609.250
NucleoSpin Plasmid Transfection-grade	MACHEREY-NAGEL	Cat# 740490.250
CellTiter-Glo Luminescent Cell Viability Assay	Promega	Cat# G7570
Live & Dead Zombie NIR Fixable Viability Kit	Biolegend	Cat# 423106
eBioscience Foxp3/Transcription Factor Staining Buffer	Invitrogen	Cat# 2344986
Nuclear and Cytoplasmic Protein Extraction Kit	Beyotime	Cat# P0028
Pierce BCA Protein Assay Kit	Thermo Scientific	Cat# 23225
T4 DNA Ligase kit	Thermo Scientific	Cat# EL0012
EZ DNA Methylation-Gold™ Kit	ZYMO research	Cat# D5005
TA/Blunt-Zero Cloning Kit	Vazyme	Cat# C601-01
PrimerSTAR™ Max	TAKARA	Cat# R045A
EpiTaq™ HS	TAKARA	Cat# R110Q
Deposited data		
Raw and analyzed data	This paper	GEO: GSE268920
Human NSCLC ICB RNA-seq dataset 1	Hwang et al.[20]	GEO: GSE136961
Human Gastric ICB RNA-seq dataset 2	Kim et al.[21]	PRJEB25780
Human ccRCC ICB RNA-seq dataset 3	Miao et al.[22]	NIHMS978739
Experimental models: Cell lines		
PBMC from healthy doners	SailyBio Technologies, Beijing, China	N/A
Homo sapiens: A498	National Collection of Authenticated Cell Cultures, Shanghai, China	RRID: CVCL_1056
Homo sapiens: SW480	National Collection of Authenticated Cell Cultures, Shanghai, China	RRID: CVCL_0546
Homo sapiens: A549	National Collection of Authenticated Cell Cultures, Shanghai, China	RRID: CVCL_0023

(*Continued on next page*)

Continued

REAGENT or RESOURCE	SOURCE	IDENTIFIER
Homo sapiens: SKBR3	National Collection of Authenticated Cell Cultures, Shanghai, China	RRID: CVCL_0033
Homo sapiens: MDA-BM-231	National Collection of Authenticated Cell Cultures, Shanghai, China	RRID: CVCL_0062
Homo sapiens: NK-92MI	Shanghai Biofeng Biotech.	RRID: CVCL_3755
Mus musculus: B16F10	National Collection of Authenticated Cell Cultures, Shanghai, China	RRID: CVCL_0159
Mus musculus: MC38	National Collection of Authenticated Cell Cultures, Shanghai, China	RRID: CVCL_B288
Mus musculus: LLC	National Collection of Authenticated Cell Cultures, Shanghai, China	RRID: CVCL_4358
Mus musculus: 4T1	National Collection of Authenticated Cell Cultures, Shanghai, China	RRID: CVCL_0125
Mus musculus: EMT6	National Collection of Authenticated Cell Cultures, Shanghai, China	RRID: CVCL_1923
Homo sapiens: FreeStyle™ 293-F	Liu et al.[32]	N/A
Mus musculus: B16F10 EGFR	Liu et al.[32]	N/A
Mus musculus: MC38 EGFR	Liu et al.[32]	N/A
Experimental models: Organisms/strains		
Mouse: C57BL/6J	Beijing Vital River Laboratory	RRID: IMSR_JAX:000664
Mouse: BALB/c	Beijing Vital River Laboratory	RRID: IMSR_JAX:000651
Mouse: NOD.Cg-Prkdcscid Il2rgtm1Wjl/SzJ (NSG)	The Jackson Laboratory	RRID: IMSR_JAX:005557
Mouse: C57BL/6-Tg(TcraTcrb)1100Mjb/J (OT-I)	The Jackson Laboratory	RRID: IMSR_JAX:003831
Mouse: B6.Cg-Thy1a/Cy Tg(TcraTcrb)8Rest/J (Pmel-1)	The Jackson Laboratory	RRID: IMSR_JAX:005023
Mouse: Rosa26-LSL-Cas9 knockin	The Jackson Laboratory	RRID: IMSR_JAX:024857
Oligonucleotides		
sgRNA sequences to generate KO cell lines, see Table S3	This paper	N/A
Primers for TIDE analysis, see Table S4	This paper	N/A
ICAM1 BSP_Fwd TTAAGTTTAGTTTGGTT GGGAAAT	This paper	http://www.urogene.org/methprimer/
ICAM1 BSP_Rev AACTCTAAATAACAAA AAAACTCAAC	This paper	http://www.urogene.org/methprimer/
Recombinant DNA		
lentiCas9-Blast	Addgene	RRID: Addgene_52962
lentiCRISPRv2-puro	Addgene	RRID: Addgene_98290
lentiCRISPRv2-hygro	Addgene	RRID: Addgene_98291
lentiCRISPRv2-eGFP	This paper	N/A
lentiCRISPRv2-tdTomato	This paper	N/A
pMYs-GFP-U6-BbsI	This paper	N/A
pHAGE-EF1aL-eGFP	Addgene	RRID: Addgene_126686
pHAGE-miniCMV-eGFP	This paper	N/A

(*Continued on next page*)

Continued

REAGENT or RESOURCE	SOURCE	IDENTIFIER
psPAX2	Addgene	RRID: Addgene_12260
pMD2.G	Addgene	RRID: Addgene_12259
Human sgRNA library Brunello in lentiGuide-Puro	Addgene	RRID: Addgene_73178
Software and algorithms		
GraphPad Prism 9	GraphPad	RRID: SCR_002798
FlowJo 10	BD	RRID: SCR_008520
STAR v2.6.1day	Dobin et al.[49]	RRID: SCR_004463
DESeq2 v1.34.0	Bioconductor	RRID: SCR_000154
methylKit	Akalin et al.[50]	RRID: SCR_005177
Seurat v5	Hao et al.[51]	RRID: SCR_016341
MaGeCK	Li et al.[52]	https://sourceforge.net/p/mageck/wiki/Home/
TIDE	Brinkman et al.[53]	https://tide.nki.nl/
QUMA	Kumaki et al.[54]	http://quma.cdb.riken.jp/top/quma_main_j.html
AlphaFold 3	Abramson et al.[55]	https://alphafold.com/

EXPERIMENTAL MODEL AND STUDY PARTICIPANT DETAILS

Cell lines

A549, MDA-BM-231, B16F10, MC38 and LLC cells were maintained in DMEM medium supplemented with 10% fetal bovine serum,100 mg/mL penicillin and 100U/mL streptomycin. A498, SW480, and 4T1 cells were maintained in RPMI 1640 medium supplemented with 10% fetal bovine serum and penicillin-streptomycin. SKBR3 cells were maintained in McCoy's 5A media supplemented with 10% fetal bovine serum, 100 mg/mL penicillin and 100U/mL streptomycin. NK-92MI cells were maintained in Alpha MEM without ribonucleosides supplemented with 1.5 g/L sodium bicarbonate, 0.2 mM Myo-inositol, 0.1 mM 2-mercaptoethanol, 0.02 mM folic acid and 12.5% fetal bovine serum and horse serum. All the cells were incubated at 37°C and 5% CO_2.

Primary cultures

Human peripheral blood mononuclear cells (PBMCs) were obtained from healthy donors (SailyBio Technologies) under the Shanghai Liquan Hospital institutional review board–approved protocol. All human participants provided written informed consent prior to their participation in the study. On day 1, $CD8^+$ T cells were isolated using the EasySep Human $CD8^+$ T cell Enrichment Isolation Kit and stimulated with precoated anti-human-CD3 (5 μg/mL), anti-human-CD28 (1 μg/mL), and human fibronectin (5 μg/mL). On day 2, lentivirus expressing the NY-ESO-1 (HA+) TCR construct was added to the 24-well plates, followed by centrifugation at 1100*g* for 2.5 h at 32°C. After infection, cells were incubated at 37°C with 5% CO_2. On day 5, NY-ESO-1 expressing T cells were sorted by FACS using anti-HA antibodies and Alexa Fluor 488 Conjugate anti-rabbit IgG (H + L), F(ab')2 Fragment. T cells were then expanded in human T cell media (RPMI 1640 media with 10% heat-inactivated fetal bovine serum, 1mM sodium pyruvate, 2mM L-glutamine, 1× NEAA, 100 mg/mL penicillin and 100U/mL streptomycin) with recombinant human IL-2 (200IU/mL).

For OT-I or Pmel-1 $CD8^+$ T cells, $CD8^+$ T cells were isolated from mouse spleens using the MojoSort Mouse $CD8^+$ T cell Isolation kit and activated using anti-mouse-CD3 (5 μg/mL) and anti-mouse-CD28 (1 μg/mL). For CD11a KO OT-1 cells, follow the same protocol for infection as human $CD8^+$ T cells. On day 5, CD11a KO T cells were sorted by FACS using anti-mouse-CD54. T cells were cultured and expanded in murine T cell media (RPMI 1640 media with 10% heat-inactivated fetal bovine serum, 20mM HEPES, 1mM sodium pyruvate, 0.05mM 2-mercaptoethanol, 2mM L-glutamine, 100 mg/mL penicillin and 100U/mL streptomycin.) with recombinant mouse IL-2 (20 ng/mL).

Mice

Six to eight-week-old C57BL/6J, BALB/c mice were purchased from Beijing Vital River Laboratory. NOD.Cg-Prkdcscid Il2rgtm1Wjl/SzJ (NSG), C57BL/6-Tg (TcraTcrb)1100Mjb/J (OT-I), B6.Cg-Thy1a/Cy Tg(TcraTcrb)8Rest/J (Pmel-1) and Rosa26-LSL-Cas9 knockin mice were purchased from The Jackson Laboratory and bred at the Laboratory Animal Resources Center of Tsinghua University. The mice were maintained in pathogen-free conditions with a 12/12-h light/dark cycle, 22°C–26°C, 30–70% relative humidity with sterile pellet food and water *ad libitum*. All mice experiments were conducted according to Institutional Animal Care and Use Committee (IACUC)–approved protocols of Tsinghua University, Beijing, China.

METHOD DETAILS

Generation of cell lines

Generation of NY-ESO-1 expressing cell lines

A498, SW480, and SKBR3 cells, all of which express the endogenous HLA-A2 allele, were infected with lentivirus expressing NY-ESO-1 antigen linked with eGFP. In the case of constructing A549-NY-ESO-1 cells, the lentiviral construct also expresses the HLA-A*02:01 heavy chain, which is necessary for presenting the NY-ESO-1 antigen to the NY-ESO-1 specific TCR used in this study.

Generation of Icam-1 *overexpressing and vector cell lines*

B16F10 and 4T1 *Icam1* overexpressing (*Icam1*^{OE}) cells were generated by lentiviral transduction of murine *Icam1*-T2A-GFP driven by a miniCMV promoter. GFP+ *Icam1* expressing cells were stained anti-mouse-CD54 then FACS sorted and used for subsequent experiments. Vector control cells were generated by lentiviral transduction of GFP vector driven by a miniCMV promoter and GFP+ cells were FACS sorted for use.

Generation of KO cell lines

The sgRNA sequences and corresponding backbone were used to generate KO cell lines were listed in Table S3. Cells were infected with lentiviruses expressing sgRNA. Two days after infection, puromycin (2 μg/mL) or hygromycin B (50 μg/mL) was added to the culture for selection of KO cell lines. For ICAM1 KO and B2M KO tumor cells were FACS sorted with following antibodies: anti-human-CD54 and anti-mouse-H2K^{d}.

FACS-based genome wide CRISPR screen

A549-Cas9 cells were generated by transfection with lentivirus encoding Cas9-Blast and selected with blasticidin (12 μg/mL). A549-Cas9 cells were then transfected with the Brunello lentivirus library at an infection rate of 10%. After 48 h of transfection, transduced cells were selected using puromycin (2 μg/mL) for 2 days. Twelve days after viral transfection, cells were stained with APC anti-human-CD54 antibody and sorted into ICAM-1^{high} and ICAM-1^{low} subsets. Genomic DNA of the sorted cells was extracted using the NucleoSpin Blood L kit following the manufacturer's protocol. Amplification of the sgRNA cassettes by PCR was performed according to the broad GPP protocol https://portals.broadinstitute.org/gpp/public/resources/protocols. MaGeCK RRA module was used to process and analyze the CRISPR screen data.

In vitro tumor with NY-ESO-1 specific CTLs or NK-92MI cells co-culture

In vitro *competition assay*

The control cells were mixed with tdTomato^{+} control or ICAM-1 KO cells at an approximate 1:1 ratio. The cell mixtures were seeded at 80% confluence in a 12-well plate. Six hours after seeding, NY-ESO-1 specific CTLs or NK-92MI cells were added at E:T ratio of 1:3 or 1:1, respectively. After 24 h of co-culture, the remaining tumor cells were collected and the ratio of mixed tumor cells was analyzed by FACS (CytoFLEX S, Beckman) and FlowJo. The following antibodies were used for gating tumor cells: (1) Human tumor-CTL co-culture assay: Live & Dead Zombie NIR Fixable Viability Kit, anti-human-CD8a; (2) Human tumor-NK-92MI co-culture assay: Live & Dead Zombie NIR Fixable Viability Kit, anti-human-CD56; (3) Murine tumor-CTL co-culture assay: DAPI, anti-mouse-CD8a, anti-mouse-CD54.

CTL and NK-92MI-mediated killing assay with anti-ICAM-1 blockade

Tumor cells were seeded at 80% confluence in a 12-well plate. Isotype control mouse IgG1 antibodies (5 μg/mL) or Anti-ICAM1 monoclonal antibodies (5 μg/mL) were added to the wells. After 30 min of incubation with the antibodies, human NY-ESO-1 specific CTLs or NK-92MI cells were added at E:T ratio of 1:3 or 1:1, respectively. After 24 h of co-culture, the remaining tumor cells were collected, and viable cells were analyzed by flow cytometry.

Human CTLs and NK-92MI cell cytotoxicity assay

Tumor cells were seeded at 80% confluence in a 12-well plate. Six hours after seeding, NY-ESO-1 specific CTLs were added at E:T ratio of 1:1 in the presence of 5 mg/mL Brefeldin A. NK-92MI cells were added at E:T ratio of 1:1. After 6 h of co-culture, NY-ESO-1 specific CTLs or NK-92MI cells were harvested then analyzed by FACS and FlowJo. The following antibodies were used: (1) NY-ESO-1 specific CTLs cytotoxicity assay: Live & Dead Zombie NIR Fixable Viability Kit, anti-human-CD8a, anti-human-IFN-γ; (2) NK-92MI cells cytotoxicity assay: Live & Dead Zombie NIR Fixable Viability Kit, anti-human-CD56, anti-human-CD107a. The cells were stained with Live & Dead Zombie NIR Fixable Viability Kit and surface markers in PBS for 15 min at room temperature. For intracellular cytokine IFN-γ staining, cells were processed using the eBioscience Foxp3/Transcription Factor Staining Buffer followed by manufacturer's instructions.

Cell proliferation assay

For cell proliferation and viability experiments, number of 100 A498 or 200 SW480 indicated tumor cells were plated in 96-well plates and alive cells were quantified using CellTiter-Glo Luminescent Cell Viability Assay Kit every 2 days. The k-value is calculated using exponential growth equation in GraphPad Prism 9 to represent the cell growth rate.

For cell competition proliferation assay, ICAM-1 KO and control tumor cells were mixture at approximately 1:1 ratio. Mixture tumor cells were cultured and ratio of alive cells were analyzed using FACS every 2 days.

Western blot

Total cell lysates or nuclear extractions were extracted by Nuclear and Cytoplasmic Protein Extraction Kit according to the manufacturer's protocol. Protein concentrations were assayed by BCA Protein assay kit and 20μg total protein or nuclear protein was loaded per lane onto 4–12% gradient, SurePAGE, Bis-Tris gels. Gels were transferred to Immobilon PVDF membranes. Membranes were blocked in TBST containing 5% skim milk for 2 h at room temperature and incubated primary antibodies overnight in 4°C and followed by IgG (H&L)-HRP conjugated secondary antibodies in room temperature for 1 h. Enhanced chemiluminescence substrates were used to visualize the specific bands on the membrane. Chemiluminescence was captured using Amersham Imager 600 (GE).

Tracking of Indels by DEcomposition (TIDE) analysis for gene editing efficiency

Genomic DNA of the target gene knockout tumor cells was extracted using the NucleoSpin Tissue, Mini kit for DNA from cells and tissue following the manufacturer's protocol. PCR amplification of a stretch of DNA ~700bp enclosing the designed editing site (sgRNA) using PrimerSTAR Max by following thermal cycling protocol, 98°C for 2min and 30 cycles each of 98°C for 10 s, 60°C for 5 s, and 72°C for 7s. Pair of PCR products from control and target gene knockout tumor cells were sequenced and upload the sequencing files on the TIDE https://tide.nki.nl/ to get the gene editing efficiency. The primers used were listed in Table S4.

Whole genome bisulfite sequencing (WGBS) and focused bisulfite sequencing of *ICAM1* promoter region

The genomic DNAs of A549 control and UHRF1 KO tumor cells were isolated using the NucleoSpin Blood Mini kit for DNA from cells and tissue. The EZ DNA Methylation-Gold Kit were used for DNA bisulfite conversion of genomic DNA (400ng) according to the manufacturers' instructions. The DNA bisulfite converted DNA were then used for WGBS and focused bisulfite sequencing. For WGBS, clean reads were mapped to human reference genome by Bismark and only uniquely mapped reads were retained. CpG methylation levels were detected with the R package ''methylKit''. Differential methylated sites were defined by a cutoff for 20 percentage of absolute change of methylation. The promoter and CpG region of indicated genes were obtained from UCSC genome table browser. For BSP, the PCR amplification of *ICAM1* promoter region was using EpiTaq HS by following thermal cycling protocol, 98°C for 2min and 40 cycles each of 98°C for 10 s, 55°C for 30 s, and 72°C for 45s. PCR products were isolated by Mini kit for Gel and PCR Clean-up and subcloned into the TA/Blunt-Zero Cloning Kit then individual clones were sequenced. The methylation status of the region was determined and analyzed with QUMA http://quma.cdb.riken.jp/top/quma_main_j.html.

In vivo animal studies xenograft mouse models

For tumor challenge, $1x10^6$ 4T1, $1x10^6$ B16F10 and $1x10^6$ MC38 cells were resuspended in PBS and injected subcutaneously (s.c.) into the flanks of mice. $0.7x10^6$ B16F10 EGFR cells were prepared and injected into NSG mice following the same protocol. For fusion protein treatment, mice bearing tumors were intratumorally/intravenously (i.t./i.v.) injected with 5 mg/kg Cetuximab or Cet×ICAM1-D1. For anti-PD1 treatment, mice bearing tumors were intraperitoneally (i.p.) injected with 5 mg/kg of anti-PD1 antibodies every three days starting from day 7 post tumor inoculation. The length and width were measured every 2–3 days when the tumors became palpable and tumor volume was calculated using the following formula: (length × $width^2$)/2. The endpoint was recorded when the tumor volume reached $2000mm^3$ or mice died. Randomization was performed on age and sex-matched mice when possible. When measuring the tumor size, investigators were blinded for sample allocations when feasible.

Flow cytometry and analysis of tumor infiltrating lymphocytes

Tumors were dissociated in gentleMACS dissociator with collagenase type IV (1 mg/mL), DNAse type IV (20 units/mL) and hyaluronidase type V (0.1 mg/mL) for 30 min at 37°C. Cells were passed through a 70-μm filter and a small fraction was used for FACS. Cells were stained with fluorophore-conjugated antibodies in PBS containing 1% fetal bovine serum. The following antibodies were used: anti-mouse-CD45, anti-mouse-CD3, anti-mouse-CD8a, anti-mouse-CD4, anti-mouse-NKp46, anti-human/mouse-Granzyme B, anti-mouse-CD62L, anti-mouse-Ly108, anti-mouse-TIM3. Cells were first stained with Live & Dead Zombie NIR Fixable Viability Kit and anti-mouse-CD16/32 in PBS for 15 min at room temperature to block the IgG Fc receptor. The cells were stained with surface markers, fixed, and permeabilized for intracellular staining with eBioscience Foxp3/Transcription Factor Staining Buffer followed by manufacturer's instructions. Beckman Coulter CytoFLEX S was used for data collection and FlowJo was used for data analysis.

Bulk RNA-seq

A549 wild-type cells were cultured in replicates, stained with anti-human-CD54 antibody, and sorted $ICAM1^{high}$ and $ICAM1^{low}$ subsets by FACS AriaIII (BD). The cells were washed with PBS and lysed using TRIzol. The reads were aligned to the GRCh38 using STAR. Feature count was used to map aligned reads to genes and generate a gene count matrix. Statistical analysis of the differentially expressed genes was performed using the DESeq2 R package.

Single cell RNA-seq of immune cells isolated from Cetuximab and Cet×ICAM1-D1 treated tumors

Single-cell suspensions were obtained from mice bearing MC38-EGFR treated with Cetuximab and Cet×ICAM1-D1 on day 14. Cells were stained with Live & DEAD Zombie NIR Fixable Viability Kit and anti-mouse-CD45. Equally numbers of alive $CD45^+$ cells were sorted by FACS AriaIII (BD) from each sample of Cetuximab and Cet×ICAM1-D1 treated tumors then pooled together, respectively. The cells were washed with PBS for library construction of scRNA-seq.

Single cell RNA-seq analysis

SingleCellExperiment (v1.16.0) was used for quality control purposes. Cells with low log-transformed library size, low log-transformed number of expressed genes, or high mitochondrial proportions that were more than 3 MADs (median absolute deviation) from the median were identified as low-quality cells and discarded. Seurat (v5) was used for integration, normalization, dimensionality reduction, clustering, UMAP visualization, and marker gene detection, based on which manual annotation was performed for each cluster. Other downstream analyses were performed using custom R (v4.1.3) scripts.

Analysis of ICB cohorts

Human ICB RNA-seq datasets[20–22] (see Table S5) are obtained from public databases. Samples were stratified by response status, and tumor ICAM-1 expression levels were compared between the responders and non-responders.

Experiments related to fusion protein

Design and production of fusion protein

Cet×ICAM1-D1 is composed of Fab fragment of Cetuximab and natural D1 domain of ICAM-1 (murine or human) fused with "LALA-PG" mutations Fc fragment. AlphaFold 3 was used to predict the potential binding between human ICAM1's natural D1 domain of Cet×hICAM1-D1 and human CD11a. These fusion proteins were generated by transient co-transfection of indicated plasmids into FreeStyle 293-F cells. The supernatant containing the fusion protein was purified using Protein A affinity chromatography according to the manufacturer's protocol. The heterogeneity was confirmed by SDS-PAGE.

Binding affinity of antibody to EGFR

All tumor cells were first stained with anti-mouse-CD16/32or Human TruStain FcX to block the IgG Fc receptor. Then, MC38 and B16F10 EGFR tumor cells tumor cells were incubated with serial dilutions of Cetuximab and Cet×ICAM1-D1 in PBS for 30 min at room temperature. Then, cells were stained followed by a fluorophore-conjugated anti-human IgG secondary antibody. Using FACS to measure the mean fluorescence intensity.

In vitro *tumor-T cells co-culture and cytotoxicity assay*

MC38 and B16F10 EGFR tumor cells pulsed with 100 ng/mL SIINFEKL peptide were co-incubated with OT-1 cells in the presence of serial dilutions of Cetuximab or Cet×ICAM1-D1 at E:T ratio of 1:1. ICAM-1 knockout and NY-ESO-1 positive A498 and SW480 tumor cells with endogenous EGFR were co-incubated with NY-ESO-1 specific T cells in the presence of serial dilutions of Cetuximab or Cet×hICAM1-D1 at E:T ratio of 1:1. Then the effector cells mediated killing assay and effector cells cytotoxicity assay were processed as described above.

QUANTIFICATION AND STATISTICAL ANALYSIS

Statistical analyses were performed by using GraphPad Prism 9 software and presented as means ± SEM. Statistical comparisons between multiple groups were determined by one-way ANOVA or two-way ANOVA with multiple comparisons. Statistical comparisons between two groups were determined by unpaired two-tailed Student's T test. $p < 0.05$ was considered statistically significant ($^{*}p < 0.05$, $^{**}p < 0.01$, $^{***}p < 0.001$ and $^{****}p < 0.0001$; ns, not significant). Statistical details for each experiment can be found in the figures and the legends. For ICB analysis (Figure 1H), p values are derived from linear regression model which uses tumor ICAM-1 expression level to predict responding status (responder vs. non-responder).